How Coverage Influences Thermodynamic and Kinetic Isotope Effects for H2/D2 Dissociative Adsorption on Transition Metals

How Coverage Influences Thermodynamic and Kinetic Isotope Effects for H₂/D₂ Dissociative Adsorption on Transition Metals

Benjamin W. J. Chen, Manos Mavrikakis*

Department of Chemical and Biological Engineering, University of Wisconsin – Madison,

Madison, WI 53706

*corresponding author emavrikakis@wisc.edu

ABSTRACT

Isotope effects greatly enhance our understanding of chemical reactions in heterogeneous catalysis. Despite their widespread use, there is limited understanding about how realistic reaction conditions, such as the coverage of surface adsorbates, affect them. Here, we study the influence of hydrogen (H) coverage on the thermodynamic and kinetic isotope effects of H₂/D₂ dissociative adsorption on the close-packed, open, and stepped surfaces of 12 transition metals: Ag, Au, Co, Cu, Fe, Ir, Ni, Re, Pd, Pt, Rh, and Ru, over a catalytically relevant temperature range. Through first-principles density functional theory calculations, we show that increasing coverage has two effects: *i)* it may change preferred adsorption sites and transition state geometries, and *ii)* it increases the vibrational frequencies of adsorbed H due to the interactions between H atoms. Empirically, isotope effects decrease in absolute value with increasing coverage for most of our studied systems, indicating a relative shift in stability in favor of the D-substituted minima and transition states. This is likely due to the consistent influence of the latter factor, which affects all structures. Higher temperatures reduce the magnitude of these decreases. Our findings provide

1

insights into the nanoscale mechanisms by which coverage influences isotope effects, which will affect how we interpret experimentally measured isotope effects. They also point towards new applications of isotope effects in catalysis, such as for quantifying the adsorbate coverages, as well as for elucidating adsorption and active sites on the surfaces of catalysts.

1.   Introduction

Isotopic substitution is a powerful tool for obtaining mechanistic information about chemical reactions at the nanoscale.[1–4] With the conceptually simple act of swapping one isotope for another in a reactant, we retain the chemical properties of the reactant but change its mass and thus also its translational, vibrational, and rotational properties, in turn leading to different reactivities and reaction rates. By analyzing how reaction rates vary and product distributions shift upon isotopic substitution, one can elucidate reaction mechanisms[5–10] and validate kinetic theories, such as improvements in transition state theory.[4,11]

There are two types of isotope effects: Kinetic Isotope Effects (KIEs), which quantify changes in *reaction rates* upon isotopic substitution; and Thermodynamic Isotope Effects (TIEs), sometimes known as equilibrium isotope effects, which quantify changes in the *equilibrium constants* of a reaction.

Analyzing experimental KIEs for reactions on surfaces can be complicated as the observed KIEs may be a convolution of the KIEs and TIEs of multiple elementary steps.[12–16] For example, the experimentally measured KIE of Fischer-Tropsch[13] and hydrogenation[16] reactions are found to be inverse (< 1) because of the inverse TIE of H_2 dissociation even though H_2 dissociation was not the rate determining step in these reactions. This is because the overall rate of reaction depends not only on rate constants, but also on the coverages of surface intermediates, which are affected

by the equilibrium constants of the relevant steps. A derivation for a simple example is shown in the Supporting Information (SI), Section S1. It is therefore valuable to know the KIEs and TIEs of individual elementary steps in a reaction mechanism. Unfortunately, it is tedious and sometimes impossible to experimentally measure TIEs and KIEs of an elementary step in isolation.

As a result, our knowledge of how the properties of a realistic surface, such as their step densities, defect densities, and adsorbate coverages can influence isotope effects is scant. The influence of coverage is especially relevant since high coverages of adsorbates often build up on surfaces during reactions.[17–21] Preferred adsorption sites, binding geometries, and binding energies can change as a function of the adsorbate coverage, which in turn may affect reaction rates and even pathways.[22–28] Isotope effects are not spared from the influence of adsorbate coverage: co-adsorbed H seems to enhance the KIE for H_2 dissociation on Ni(100),[29] and subsurface H decreases experimentally-observed KIEs for H_2 desorption from Ru(0001).[30] These preliminary works point to a potential range of impacts coverage may have on the isotope effects of H_2 dissociation, which will be propagated to the overall KIE—complicating their interpretation—for reactions involving H such as hydrogenations and dehydrogenations.

Here, we study how surface coverage influences isotope effects of H_2/D_2 dissociative adsorption on transition metal surfaces. We aim to shed light into how isotope effects can be affected by realistic reaction conditions, and to aid in interpretation of experimentally observed isotope effects. We perform first-principles calculations to evaluate TIEs at a coverage of 1 monolayer of H (1 ML H) for 12 close-packed (111), (110), and (0001) surfaces; 8 open (100) surfaces; and 8 stepped (211) surfaces of Ag, Au, Cu, Co, Fe, Ir, Ni, Re, Pd, Pt, Rh, and Ru. We also evaluate KIEs at the same coverage for the (111), (100), and (211) surfaces of Au, Ag, and Cu. We then compare these isotope effects with those calculated at a coverage of 1/9 ML for the TIEs and 2/9 ML for the

KIEs.[31] These comparisons are conducted under base conditions of a temperature of 623 K and a H$_2$ pressure of 0.1 atm. Since isotope effects may change under different experimental conditions, we lastly determine how varying temperature and pressure affect our results.

2.   Methods

2.1.   Density Functional Theory (DFT)-Based Calculations

Periodic, plane-wave, density functional theory (DFT)-based calculations were performed using the Vienna *ab initio* Simulation Package (VASP)[32,33]. Nuclei and core electrons were represented by projector augmented-wave (PAW) pseudopotentials[34,35], whereas the valence electron wavefunctions were expanded using a plane-wave basis set with a kinetic energy cutoff of 400 eV. The Perdew and Wang (PW91) form of the generalized gradient approximation (GGA) was used to describe contributions from exchange and correlation.[36] For Co, Ni, and Fe surfaces only, spin-polarized calculations were performed. Structures were fully relaxed until the Hellmann–Feynman forces acting on the atoms were smaller than 0.02 eV / Å. All settings were chosen for consistency with our previous publication.[31] Transition states were located with the climbing image nudged elastic band (CI–NEB) method[37] using a minimum of seven interpolated images between the initial and final states, and were confirmed to possess only one vibrational mode with an imaginary frequency.

Harmonic vibrational frequencies were calculated by first building up the Hessian via numerical differentiation of the energies using a second-order finite difference approach with a step size of 0.015 Å. The Hessian was then mass-weighted and diagonalized to yield the normal mode frequencies. The frequencies were tested for convergence with respect to the step size. For all frequency calculations, all slab atoms were fixed while all adsorbate atoms were relaxed.

Close-packed surfaces (fcc(111), hcp(0001), and bcc(110)) were modeled by five-layer 3×3 slabs, whereas open surfaces (fcc(100)) were modeled by six-layer 3×3 slabs, and stepped (fcc(211)) surfaces were modeled by a twelve-layer, 1×3 slab. The top three, four, and seven layers of the close-packed, open, and stepped surfaces respectively were allowed to relax; the rest of the layers were fixed at their bulk lattice positions, with lattice constants of (experimental values[38] in parenthesis, all values in Å): Ag $-$ 4.16 (4.09), Au $-$ 4.18 (4.08), Co $-$ a: 2.50 (2.51), c: 4.03 (4.07), Cu $-$ 3.64 (3.61), Fe $-$ 2.84 (2.87), Ir $-$ 3.88 (3.84), Ni $-$ 3.53 (3.52), Pd $-$ 3.96 (3.89), Pt $-$ 3.98 (3.92), Re $-$ a: 2.78 (2.76), c: 4.48 (4.46), Rh $-$ 3.84 (3.80), Ru $-$ a: 2.73 (2.71), c: 4.31 (4.28).

For the open (100) surfaces, we also considered a six-layer 4×4 slab to capture the symmetry of the p4g reconstruction, which is highly thermodynamically favorable for Cu(100).[39–42] We verified that the average H binding energies (BEs) for the 3×3 and 4×4 unit cells differed by < 0.01 eV and thus the results for these two unit cell sizes are practically identical.

A $6 \times 6 \times 1$ Monkhorst-Pack k-point mesh[43] was used to sample the first Brillouin zone of the close-packed and open surfaces except for Cu(111), Ag(111), and Au(111), where a finer $8 \times 8 \times 1$ Monkhorst-Pack k-point mesh was used. An $8 \times 6 \times 1$ Monkhorst-Pack k-point mesh was used for the stepped (211) surfaces. Periodic images of the slabs were separated by a vacuum region of ~12 Å in the z-direction. Adsorbates were placed on only one side of the slabs, with the electrostatic potential adjusted accordingly to prevent spurious interactions between the images.[44,45]

2.2.   Binding Energy Definitions

We define the *average* binding energy ($\overline{BE}$), applicable to both minima and transition states, as:

$$\overline{BE} = \frac{E_{\text{ads}} - E_{\text{clean}} - nE_{\text{H}}}{n}, \#(1)$$

where E_{ads}, E_{clean}, E_H are the total energies of a minimum or transition state structure, the clean slab, and the gas-phase H atom, respectively. n is the number of H atoms in the system. Negative BEs reflect exothermic binding, whereas positive BEs reflect endothermic binding.

We define the *average* zero-point energy $(\overline{ZPE})$ of a system as:

$$\overline{ZPE} = \frac{ZPE}{n} \,,\#(2)$$

where ZPE is the total ZPE of the system.

We finally define the activation energy (E_a) for a system as:

$$E_a = E_{TS} - E_{initial} - E_{H_2} \,,\#(3)$$

where E_{TS} is the total energy of a transition state structure, $E_{initial}$ is the initial state of the slab, which could be clean or covered with spectator H, and E_{H_2} is the energy of gas-phase H_2.

2.3. Calculation of Kinetic and Thermodynamic Isotope Effects

We define H_2 dissociative adsorption as the reaction: $H_2 (g) \rightarrow 2\,H^*$, where (g) denotes gas-phase species, and * denotes adsorbed species. D_2 dissociative adsorption is defined analogously, with H replaced by D.

The thermodynamic isotope effect (TIE) for H_2/D_2 dissociative adsorption is defined as:

$$TIE = \frac{K_H}{K_D} = \frac{\exp\left(-\dfrac{\Delta G_H}{RT}\right)}{\exp\left(-\dfrac{\Delta G_D}{RT}\right)} = \exp\left(-\frac{\Delta G_H - \Delta G_D}{RT}\right) = \exp\left(-\frac{\Delta H_H - \Delta H_D}{RT} + \frac{\Delta S_H - \Delta S_D}{R}\right), \#(4)$$

where K is the equilibrium constant, ΔG is the Gibbs free energy of reaction, ΔH is the enthalpy of reaction, ΔS is the entropy of reaction, R is the molar gas constant, and T is the temperature. Subscripts H and D denote quantities evaluated using the respective isotopes.

Note that the binding energies of H-metal and D-metal bonds are identical because H and D have the same electronic structure. If we approximate finite-temperature corrections to the enthalpy as negligible, as was done in our previous work,[13,31] the TIE is then:

$$TIE = \exp\left(-\frac{\Delta H_H - \Delta H_D}{RT} + \frac{\Delta S_H - \Delta S_D}{R}\right)$$

$$\approx \exp\left(-\frac{\Delta ZPE_H - \Delta ZPE_D}{RT} + \frac{\Delta S_H - \Delta S_D}{R}\right)$$

$$= \exp\left(-\frac{\Delta ZPE_H - \Delta ZPE_D}{RT}\right)$$
$$\exp\left(\frac{\Delta S_H - \Delta S_D}{R}\right) \equiv TIE_{ZPE}TIE_{Entropy} , \qquad\qquad \#\#\#\#\#\#(5)\ \#\#\#$$

where ΔZPE is the Zero Point Energy (ZPE) change of reaction, and TIE_{ZPE} and $TIE_{Entropy}$ are the ZPE and entropic contributions to the TIE respectively.

To calculate the TIE at high coverage, we consider the initial state to be a clean slab and the final state a structure with 1 ML H. All reaction quantities are averaged by the number of H_2 molecules needed to obtain the final state from the initial state. Although it would be ideal to calculate differential reaction quantities instead of averaged ones, the computational cost to do so over the entire coverage range would be prohibitive. Additionally, our averaged values can also be easily compared to experiments which measure integral properties e.g. integral heats of adsorption.

The kinetic isotope effect (KIE) for H_2/D_2 dissociative adsorption is defined similarly:

7

$$KIE = \frac{k_H}{k_D} = \frac{\exp\left(-\dfrac{\Delta G_H^{\ddagger}}{RT}\right)}{\exp\left(-\dfrac{\Delta G_D^{\ddagger}}{RT}\right)} = \exp\left(-\frac{\Delta G_H^{\ddagger} - \Delta G_D^{\ddagger}}{RT}\right) = \exp\left(-\frac{\Delta H_H^{\ddagger} - \Delta H_D^{\ddagger}}{RT} + \frac{\Delta S_H^{\ddagger} - \Delta S_D^{\ddagger}}{R}\right) \#, (6)$$

where k is the rate constant, $\Delta G^{\ddagger}$ is the Gibbs free energy of activation, $\Delta H^{\ddagger}$ is the enthalpy of activation, and $\Delta S^{\ddagger}$ is the entropy of activation, all for the dissociative adsorption reaction.

As with the TIE, we approximate finite-temperature corrections to the enthalpy as negligible. Consequently, the KIE is:

$$KIE = \exp\left(-\frac{\Delta H_H^{\ddagger} - \Delta H_D^{\ddagger}}{RT} + \frac{\Delta S_H^{\ddagger} - \Delta S_D^{\ddagger}}{R}\right)$$

$$\approx \exp\left(-\frac{\Delta ZPE_H^{\ddagger} - \Delta ZPE_D^{\ddagger}}{RT} + \frac{\Delta S_H^{\ddagger} - \Delta S_D^{\ddagger}}{R}\right)$$

$$= \exp\left(-\frac{\Delta ZPE_H^{\ddagger} - \Delta ZPE_D^{\ddagger}}{RT}\right)\exp\left(\frac{\Delta S_H^{\ddagger} - \Delta S_D^{\ddagger}}{R}\right) \equiv KIE_{ZPE}KIE_{Entropy}, \quad (7)$$

where $\Delta ZPE^{\ddagger}$ is the activation ZPE, and KIE_{ZPE} and $KIE_{Entropy}$ are the ZPE and entropic contributions to the KIE, respectively.

To calculate the KIE at high coverage, we considered as the initial state a 7/9 ML H structure, created by removing two H atoms from a 1 ML H structure to form two adjacent vacancies (seven adsorbed H atoms in the 3×3 unit cell), and as the final state the corresponding 1 ML H structure (nine adsorbed H atoms in the 3×3 unit cell). Multiple possible initial states were constructed from the non-exhaustive permutations of two adjacent vacancies in multiple final state structures. It is not possible to use a clean slab as the initial state and a structure with 1 ML H as the final state

(like we did for the calculation of the high coverage TIEs) for the calculation of the high coverage KIE. This would involve averaging all reaction quantities by the number of H_2 molecules needed to obtain the final state from the initial state, resulting in a KIE that would be convoluted with TIEs arising from the contributions of the spectator H.

Section S2 of the Supporting Information (SI) details how the ZPE and entropy of the various components of our systems are calculated. We use the harmonic oscillator approximation to calculate entropies from our vibrational frequencies. State-of-the-art methods for calculating entropies, via constructing potential energy surfaces for example, may also be used for this purpose.[46,47] Note that we neglect quantum tunneling effects in our calculations of isotope effects as such effects are expected to be significant only at temperatures < 200 K[48,49], and not at the catalytically relevant temperatures that we wish to probe in this study.

DFT-calculated frequencies have errors ranging from $3 - 5\%$, depending on the functional.[50] To test how robust our calculated isotope effects are with respect to errors in frequencies, we simulated how these errors would propagate into our calculated isotope effects for the most stable low coverage states on the 12 close-packed metal surfaces. In our analysis, we multiply the frequencies by random scaling factors drawn from a normal distribution centered on 1.00 with a standard deviation of 0.015 (Figure S2a) and recalculated the isotope effects with these scaled frequencies. Repeating this 2000 times, we obtain an ensemble of isotope effects (Figure S2b-c), which turn out to have normal distributions with standard deviations of 0.011–0.015 (Figure S2c), much smaller than the typical effects of coverage on the isotope effects (averaging 0.14 in magnitude, as shown later). This shows that our results are robust to errors in calculated frequencies.

3.   Results

To elucidate the influence of coverage on isotope effects, we compare the thermodynamic and kinetic isotope effects (TIEs and KIEs) for H_2/D_2 dissociative adsorption at high (1 monolayer (ML)) versus low (1/9 ML for TIEs and 2/9 ML for KIEs) hydrogen coverages. Data for the latter were obtained from our previous publication[31]. For the TIEs, we probe multiple H adlayer structures on the close-packed, open, and stepped surfaces of up to 12 transition metals. For the KIEs, we probe multiple transition states on the close-packed, open, and stepped surfaces of Ag, Au, and Cu. This allows us to gather a range of possible TIEs and KIEs, out of which we will focus on those resulting from the most stable minimum energy structures and transition states.

We evaluate all TIEs and KIEs at 623 K and 0.1 atm H_2/D_2 pressure for consistency with our previous publication[31], except for in the last subsection, where we analyze how our results vary with temperature. Compared with our previous publication, there are small changes (0.01 − 0.02) in TIEs and KIEs of the low-coverage structures due to rounding errors in intermediate quantities, which in our current work have been eliminated.

We do not claim that either 1/9 ML or 1 ML is the equilibrium coverage of H on any of the metal surfaces at the considered temperature and pressure. Our aim in this contribution is to analyze changes in isotope effects with changes in coverage, and not to determine absolute coverages and isotope effects values at these conditions. Our calculated isotope effect values, which span from the low to the saturation coverage regime for a given metal, are intended as useful metrics for comparing against realistic experimental data over a range of conditions.

3.1. Thermodynamic Isotope Effects of H_2/D_2 Dissociative Adsorption

3.1.1.   Close-packed Surfaces
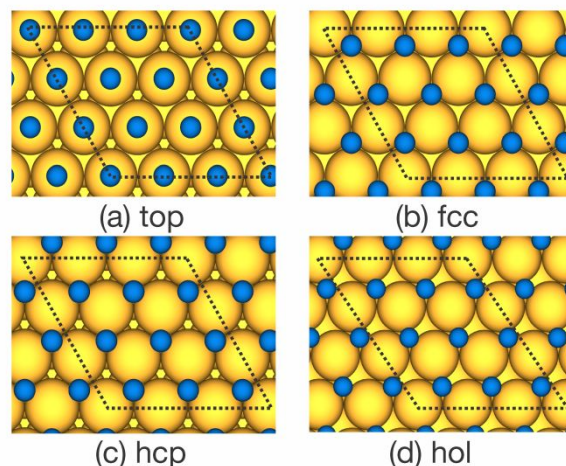
Figure 1 Top view of 1 monolayer H adlayer structures on close-packed (a-c) fcc (111) surfaces, and (d) bcc (110) surfaces. Structures are named by the sites on which H is adsorbed. In (d), "hol" is short for hollow. Adlayer structures for hcp (0001) surfaces are similar to those for fcc (111) surfaces. The unit cell is marked by dashed lines. Color code: yellow – metal, blue – H

Figure 1 illustrates the stable, high-coverage H adlayer structures we identified on the fcc (111) surfaces of Ag, Au, Cu, Ir, Ni, Pd, Pt, and Rh, the hcp (0001) surfaces of Co, Re, and Ru, and the bcc (110) surface of Fe. In these structures, H occupies all equivalent high-symmetry sites of each of the top, fcc, and hcp site types of the (111) and (0001) surfaces, and the hollow (hol) site types of the (110) surface. We omitted adlayers with mixed binding site types as there are no reports we know of that propose such structures on close-packed surfaces. Low-coverage structures involve single H atoms binding on the various high-symmetry site types, illustrations of which are shown in Figure S1a-c for the (111), (0001), and (110) surfaces respectively.

Table 1 displays thermodynamic properties and TIEs for H_2/D_2 dissociative adsorption associated with these structures. Table entries are ordered by stability; those which are most stable, having the largest absolute average zero-point-energy-corrected binding energy $(\overline{BE} + \overline{ZPE_H})$, come first. Calculated vibrational frequencies for high- and low-coverage structures can be found in Table S1.

Table 1 Calculated thermodynamic properties for H/D adsorption at 623 K and 0.1 atm H$_2$/D$_2$ pressure on close-packed surfaces, arranged in alphabetical order. Properties include average binding energies ($\overline{BE}$, eV), average zero-point energy corrected binding energies ($\overline{BE} + \overline{ZPE}$, eV), average zero-point energies ($\overline{ZPE}$, eV), and ZPE (TIE$_{ZPE}$) and entropic contributions (TIE$_{Entropy}$) to the overall thermodynamic isotope effect (TIE). See Methods for the definitions of these terms. For each surface and coverage, only stable structures are shown, and the entries are ordered by $\overline{BE} + \overline{ZPE}_H$, with the most stable states first.

| Surface | Coverage / ML | Structure | Average Binding Energies / eV | | | Average ZPEs / eV | | TIE Values | | |
			$\overline{BE}$	$\overline{BE} + \overline{ZPE}_H$	$\overline{BE} + \overline{ZPE}_D$	ZPE_H	ZPE_D	TIE$_{ZPE}$	TIE$_{Entropy}$	TIE
Ag(111)	0.11	fcc	-2.12	-1.98	-2.03	0.141	0.099	0.93	1.00	0.93
		hcp	-2.12	-1.98	-2.02	0.139	0.099	0.94	1.00	0.94
	1.00	fcc	-2.07	-1.90	-1.95	0.171	0.121	0.67	1.15	0.77
		hcp	-2.06	-1.89	-1.94	0.169	0.120	0.68	1.14	0.77
Au(111)	0.11	fcc	-2.10	-1.97	-2.00	0.129	0.091	1.05	0.95	1.00
		hcp	-2.07	-1.94	-1.98	0.126	0.089	1.09	0.94	1.03
		top	-1.91	-1.75	-1.80	0.154	0.109	0.80	1.16	0.93
	1.00	fcc	-2.02	-1.87	-1.91	0.148	0.105	0.85	1.04	0.88
		hcp	-2.01	-1.86	-1.90	0.146	0.103	0.88	1.03	0.90
		top	-1.70	-1.55	-1.60	0.154	0.109	0.80	1.16	0.93
Co(0001	0.11	fcc	-2.83	-2.65	-2.71	0.179	0.127	0.61	1.20	0.73
		hcp	-2.80	-2.63	-2.68	0.173	0.122	0.65	1.16	0.76
	1.00	fcc	-2.78	-2.58	-2.64	0.200	0.141	0.49	1.32	0.64
		hcp	-2.77	-2.57	-2.63	0.195	0.138	0.51	1.29	0.66
Cu(111)	0.11	fcc	-2.50	-2.33	-2.38	0.168	0.119	0.69	1.13	0.78
		hcp	-2.50	-2.33	-2.38	0.168	0.119	0.69	1.13	0.78
	1.00	fcc	-2.41	-2.21	-2.27	0.199	0.141	0.49	1.32	0.65
		hcp	-2.41	-2.21	-2.27	0.198	0.140	0.50	1.31	0.65
Fe(110)	0.11	hol	-3.00	-2.82	-2.87	0.171	0.121	0.67	1.15	0.77
	1.00	hol	-2.93	-2.74	-2.79	0.191	0.135	0.54	1.27	0.68
Ir(111)	0.11	top	-2.78	-2.60	-2.65	0.185	0.131	0.57	1.26	0.72
		fcc	-2.71	-2.57	-2.61	0.146	0.104	0.87	1.04	0.90
		hcp	-2.68	-2.54	-2.58	0.139	0.098	0.95	1.01	0.96
	1.00	top	-2.72	-2.53	-2.59	0.193	0.136	0.52	1.29	0.68

12

		fcc	-2.62	-2.47	-2.52	0.149	0.105	0.85	1.06	0.89
		hcp	-2.61	-2.47	-2.51	0.141	0.100	0.93	1.03	0.95
		bri	-2.60	-2.45	-2.49	0.149	0.105	0.85	1.08	0.91
Ni(111)	0.11	fcc	-2.83	-2.65	-2.70	0.179	0.127	0.61	1.19	0.73
		hcp	-2.82	-2.64	-2.69	0.177	0.125	0.63	1.18	0.74
	1.00	fcc	-2.82	-2.62	-2.68	0.202	0.143	0.48	1.34	0.64
		hcp	-2.81	-2.61	-2.67	0.199	0.141	0.49	1.32	0.65
Pd(111)	0.11	fcc	-2.87	-2.70	-2.75	0.165	0.117	0.71	1.12	0.79
		hcp	-2.82	-2.66	-2.71	0.162	0.115	0.73	1.10	0.81
	1.00	fcc	-2.81	-2.63	-2.68	0.174	0.123	0.64	1.17	0.75
		hcp	-2.75	-2.58	-2.63	0.170	0.120	0.67	1.14	0.77
Pt(111)	0.11	fcc	-2.76	-2.62	-2.66	0.142	0.101	0.91	1.02	0.92
		hcp	-2.71	-2.58	-2.62	0.134	0.095	1.00	0.99	0.99
		top	-2.76	-2.58	-2.63	0.188	0.133	0.55	1.28	0.71
	1.00	fcc	-2.71	-2.55	-2.60	0.152	0.107	0.82	1.06	0.87
		hcp	-2.66	-2.51	-2.56	0.146	0.103	0.87	1.04	0.91
		top	-2.69	-2.50	-2.55	0.192	0.136	0.53	1.29	0.68
Re(0001)	0.11	fcc	-2.97	-2.78	-2.83	0.189	0.133	0.55	1.25	0.69
		hcp	-2.93	-2.75	-2.81	0.180	0.127	0.60	1.20	0.72
	1.00	fcc	-2.82	-2.63	-2.68	0.195	0.138	0.51	1.29	0.66
		hcp	-2.80	-2.61	-2.67	0.184	0.130	0.58	1.23	0.71
Rh(111)	0.11	fcc	-2.84	-2.68	-2.72	0.162	0.115	0.74	1.11	0.81
		hcp	-2.81	-2.65	-2.70	0.157	0.111	0.77	1.08	0.84
		top	-2.49	-2.34	-2.39	0.144	0.102	0.89	1.15	1.03
	1.00	fcc	-2.79	-2.61	-2.66	0.171	0.121	0.67	1.15	0.77
		hcp	-2.76	-2.60	-2.65	0.167	0.118	0.70	1.13	0.79
Ru(0001	0.11	fcc	-2.89	-2.73	-2.78	0.167	0.118	0.69	1.13	0.79
		hcp	-2.82	-2.66	-2.71	0.158	0.111	0.77	1.08	0.84
		top	-2.44	-2.31	-2.35	0.130	0.092	1.04	1.11	1.15
	1.00	fcc	-2.84	-2.66	-2.72	0.179	0.127	0.61	1.20	0.73
		hcp	-2.80	-2.63	-2.68	0.175	0.123	0.64	1.17	0.75
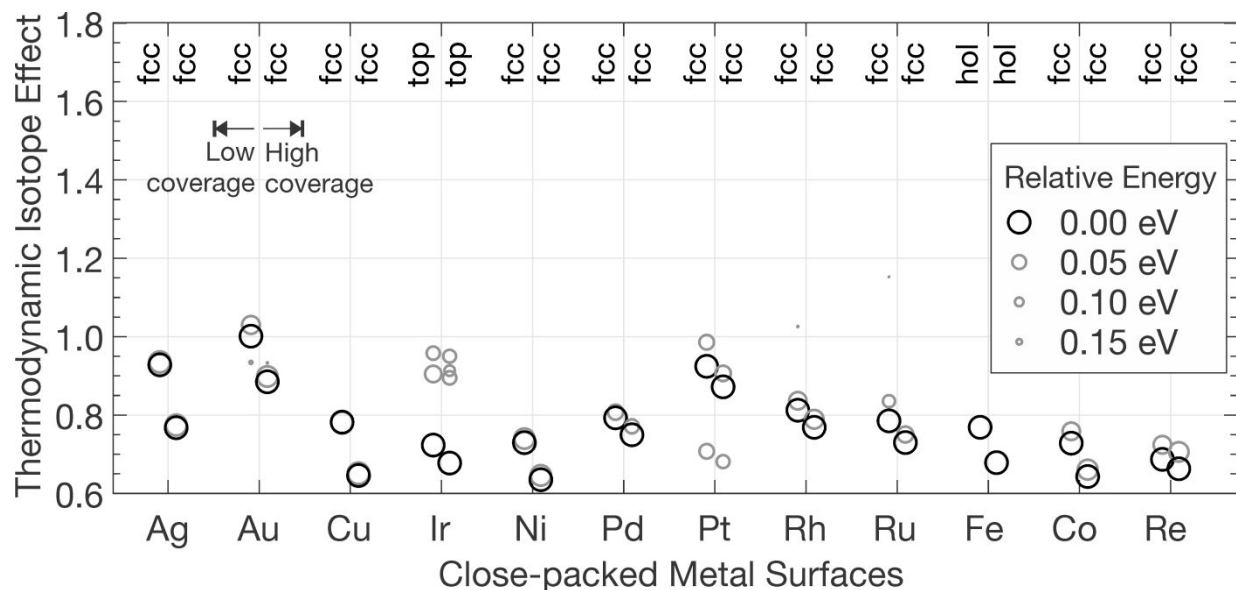
Figure 2 Calculated thermodynamic isotope effects (TIEs) for H_2/D_2 dissociative adsorption on close-packed surfaces. Circles mark the TIE for each calculated structure in Table 1. For each metal, the left-most data points correspond to the low coverage (1/9 ML) TIEs; the right-most data points correspond to the high coverage (1 ML) TIEs. Larger circles reflect more stable structures; the circles sizes are based on a Boltzmann distribution at 623 K. The most stable structures for each surface and coverage are highlighted in black and are labelled by their names at the top *x*-axis. All TIEs are evaluated at 623 K and 0.1 atm H_2/D_2 pressure.

Comparing the high and low coverage adsorption structures, there are no changes in the adsorption site preferences of H with increasing coverage (Table 1). Our calculated site preferences of H on these surfaces are in agreement with experimental findings on the close-packed surfaces of Ru[51], Ag[52], Cu[53] Pt,[54], Pd,[55], Ir[56], Rh[57], Fe[58], Co[59], and Ni[58], and in agreement with theory for Au[60] and Re[60], for which we did not find any experimental reports.

We plot a comparison of the high and low-coverage TIEs in Figure 2. Comparing only the most stable adlayer structures at low and high coverages, the TIEs decrease with increasing coverage for all metal surfaces by an average of 0.08 (Table 1 and Figure 2). Since there are no changes in the binding preferences of H, these decreases in the TIE must thus be induced by changes in the vibrational frequencies of the metal-H bonds. This is because the TIE at a constant temperature is only affected by changes in zero-point energy (ZPE) and entropy (Equation 4) — both of which

are dependent only on the vibrational frequencies of a system. The effect of these changes in vibrational frequencies always decreases the TIE, as observed by comparing all pairs of structures (not just the most stable ones) with the same H adsorption sites at high and low coverage (Table 1).

Direct comparison of the vibrational frequencies of the low- and high-coverage structures is difficult as there are more adsorbates and thus more vibrational modes at high coverage. Changes in the average ZPE of a structure are however good proxies for the changes in vibrational frequencies that occur with increasing coverage. The larger average ZPEs of the high coverage structures (by 0.01 - 0.02 eV) compared with the low coverage structures (Table 1; Figure S2) indicate that increasing coverage shifts the vibrational frequencies of the adsorbates *higher*, in agreement with the literature[22,61–63]. These increases are due to destabilizing interactions between H adatoms, which create steeper potential energy wells and more corrugated potential energy surfaces for H adsorption.[62]

The higher vibrational frequencies induced by increasing adsorbate coverage decrease the TIE, i.e. they destabilize adsorbed H relative to adsorbed D. We indeed find a good inverse correlation between the TIE and the average ZPE per H atom (Figure S3). To understand why, we break the TIE down into its ZPE and entropic contributions and track how higher frequencies affect each component. The ZPE differences between adsorbed H and D increase with higher vibrational frequencies, and because H has larger ZPEs than D, this *destabilizes* H more and leads to a *decrease* in the ZPE contributions to the TIE. The entropy differences between H and D however decrease with higher vibrational frequencies as the excited vibrational levels become harder to occupy. As D always has larger vibrational entropy, this decrease *stabilizes* H relative to D, and leads to an *increase* in the entropic contributions to the TIE. These trends are reflected in Table 1;

the high-coverage TIEs have larger entropic contributions and smaller ZPE contributions compared to the low-coverage ones. For our systems, and at the considered temperature, the decrease in ZPE contributions is larger than the increase in entropic contributions, thus the overall effect is a decrease in the TIE.

Comparing the different surfaces, weakly binding surfaces tend to exhibit larger TIEs. For example, Au and Ag have TIEs of 1.00 and 0.93 respectively at 1/9 ML coverage, whereas most other surfaces have TIEs lower than 0.9 at the same coverage (Table 1). This can be explained by the smaller vibrational frequencies of H on these surfaces, which are in turn because these surfaces bind H much weaker than others at the same coverage.[64] These smaller vibrational frequencies translate into larger TIEs, as explained above.

3.1.2.   Open Surfaces
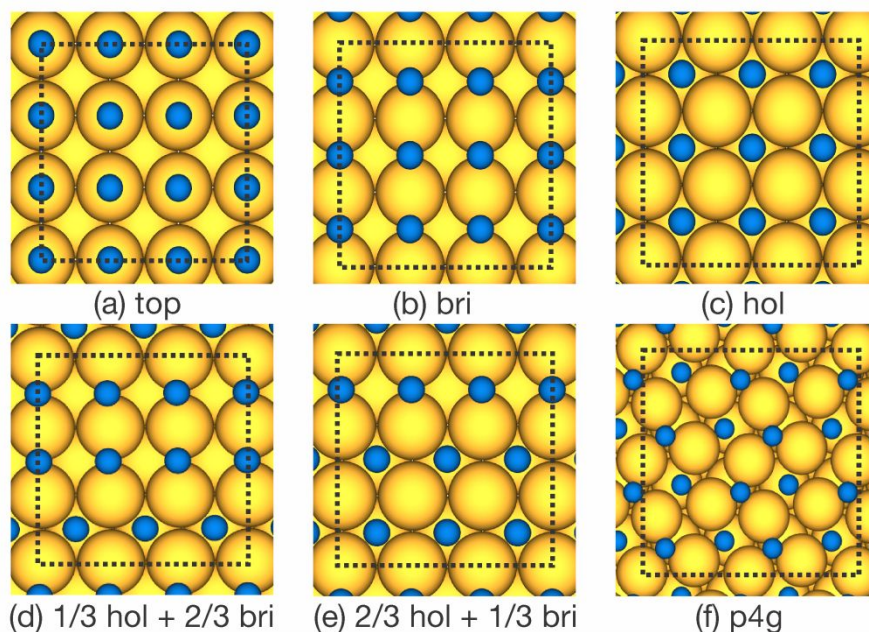
Figure 3 Top view of 1 monolayer H adlayer structures on open fcc (100) surfaces. Structures are named by the sites on which H is adsorbed. See main text for explanations of structure names. The unit cell is marked by dashed lines. Color code: yellow – metal, blue – H.

Figure 3 illustrates the six high-coverage adlayer structures we identified for 1 ML H adsorbed on the open fcc (100) surfaces of Ag, Au, Cu, Ir, Ni, Pd, Pt, and Rh. In these structures, H binds on *i)* all top sites (top); *ii)* all bridge sites (bri); *iii)* all hollow sites (hol); *iv)* 1/3 hollow sites and 2/3 bridge sites (1/3 hol + 2/3 bri); *v)* 2/3 hollow sites and 1/3 bridge sites (2/3 hol + 1/3 bri); and *vi)* the hollow sites of a H-induced p4g reconstruction (p4g). Low-coverage structures involve single H atoms binding at various high-symmetry site types on the (100) surface, illustrations of which are shown in Figure S1d.

Table 2 displays thermodynamic properties and TIEs for H_2/D_2 dissociative adsorption associated with these structures. For each metal, table entries are ordered by stability; those which are most stable, having the largest absolute $\overline{BE} + \overline{ZPE_H}$, come first. Vibrational frequencies of the high and low coverage structures can be found in Table S2.

Table 2 Calculated thermodynamic properties for H/D adsorption at 623 K and 0.1 atm H_2/D_2 pressure on open surfaces, arranged in alphabetical order. Properties include average binding energies ($\overline{BE}$, eV), average zero-point energy corrected binding energies ($\overline{BE} + \overline{ZPE}$, eV), average zero-point energies ($\overline{ZPE}$, eV), and ZPE (TIE_{ZPE}) and entropic contributions ($TIE_{Entropy}$) to the overall thermodynamic isotope effect (TIE). See Methods for the definitions of these terms. For each surface and coverage, only stable structures are shown, and the entries are ordered by $\overline{BE} + \overline{ZPE}_H$, with the most stable states first.

Surface	Coverage / ML	Structure	Average BEs / eV			Average ZPEs / eV		TIE Values		
			$\overline{BE}$	$\overline{BE} + \overline{ZPE}_H$	$\overline{BE} + \overline{ZPE}_D$	$\overline{ZPE}_H$	$\overline{ZPE}_D$	TIE_{ZPE}	$TIE_{Entropy}$	TIE
Ag(100)	0.11	hol	-1.96	-1.89	-1.91	0.069	0.049	2.03	0.78	1.59
		bri	-1.96	-1.82	-1.86	0.140	0.099	0.93	1.07	0.99
	1.00	p4g	-2.04	-1.90	-1.94	0.140	0.099	0.93	1.02	0.95
		1/3hol+2/3bri	-1.97	-1.82	-1.87	0.141	0.100	0.92	1.04	0.96
Au(100)	0.11	bri	-2.22	-2.06	-2.11	0.158	0.112	0.77	1.12	0.86
		top	-1.92	-1.78	-1.82	0.143	0.101	0.90	1.15	1.04
	1.00	bri	-2.17	-2.00	-2.05	0.166	0.118	0.70	1.16	0.81
Cu(100)	0.11	hol	-2.41	-2.30	-2.33	0.107	0.075	1.34	0.87	1.17
		bri	-2.31	-2.15	-2.20	0.157	0.111	0.78	1.16	0.90
	1.00	p4g	-2.36	-2.20	-2.25	0.162	0.114	0.74	1.11	0.82
		hol	-2.32	-2.20	-2.23	0.115	0.081	1.23	0.91	1.12
		2/3hol+1/3bri	-2.31	-2.17	-2.21	0.144	0.102	0.89	1.04	0.93
		1/3hol+2/3bri	-2.28	-2.12	-2.17	0.164	0.116	0.71	1.15	0.82
Ir(100)	0.11	bri	-2.95	-2.78	-2.83	0.168	0.118	0.69	1.16	0.81
		top	-2.87	-2.70	-2.75	0.171	0.121	0.67	1.22	0.81
	1.00	bri	-2.98	-2.81	-2.86	0.175	0.124	0.63	1.20	0.76
		top	-2.82	-2.64	-2.69	0.180	0.127	0.60	1.25	0.75
Ni(100)	0.11	hol	-2.77	-2.66	-2.69	0.164	0.116	1.28	0.89	1.14
		bri	-2.69	-2.52	-2.57	0.111	0.078	0.72	1.20	0.86
	1.00	hol	-2.83	-2.70	-2.74	0.132	0.093	1.02	0.97	0.98
		2/3hol+1/3bri	-2.77	-2.62	-2.67	0.149	0.105	0.84	1.06	0.89
Pd(100)	0.11	hol	-2.75	-2.69	-2.71	0.061	0.043	2.21	0.78	1.72
		bri	-2.76	-2.60	-2.64	0.164	0.116	0.72	1.19	0.85
	1.00	hol	-2.79	-2.70	-2.73	0.086	0.061	1.68	0.82	1.37
		2/3hol+1/3bri	-2.75	-2.64	-2.67	0.113	0.080	1.25	0.93	1.16

		1/3hol+2/3bri	-2.71	-2.58	-2.62	0.137	0.097	0.96	1.04	1.01
		bri	-2.69	-2.52	-2.57	0.167	0.118	0.70	1.19	0.83
Pt(100)	0.11	bri	-2.95	-2.78	-2.83	0.170	0.121	0.67	1.19	0.79
		top	-2.75	-2.58	-2.63	0.165	0.117	0.71	1.22	0.87
	1.00	bri	-2.93	-2.76	-2.81	0.173	0.122	0.65	1.19	0.78
		top	-2.68	-2.51	-2.56	0.165	0.117	0.71	1.22	0.86
Rh(100)	0.11	hol	-2.77	-2.69	-2.71	0.074	0.053	1.91	0.81	1.55
		bri	-2.79	-2.64	-2.68	0.158	0.112	0.77	1.14	0.88
	1.00	2/3hol+1/3bri	-2.77	-2.65	-2.69	0.119	0.084	1.18	0.94	1.11
		1/3hol+2/3bri	-2.77	-2.63	-2.67	0.140	0.099	0.93	1.04	0.97
		bri	-2.77	-2.61	-2.65	0.165	0.117	0.71	1.16	0.82

.
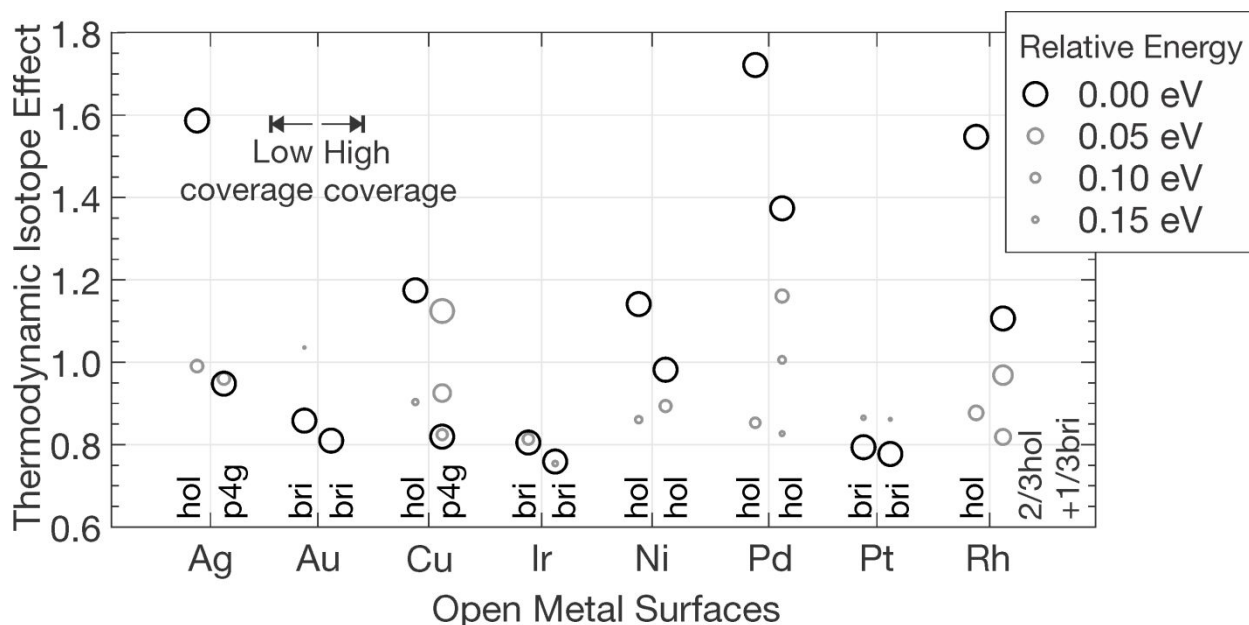
Figure 4 Calculated thermodynamic isotope effects (TIEs) for H_2/D_2 dissociative adsorption on open surfaces. Circles mark the TIE for each calculated structure in Table 2. For each metal, the left-most data points correspond to the low coverage (1/9 ML) TIEs; the right-most data points correspond to the high coverage (1 ML) TIEs. Larger circles reflect more stable structures; the circles sizes are based on a Boltzmann distribution at 623 K. The most stable structures for each surface and coverage are highlighted in black and are labelled by their names at the top *x*-axis. All TIEs are evaluated at 623 K and 0.1 atm H_2/D_2 pressure.

For all surfaces except Ag(100), Cu(100), and Rh(100), the preferred H adsorption site does not

change upon increasing coverage (Table 2). Our predicted site binding preferences are consistent

with experiments for Ir[65], Ni[66], Pd[67], and Pt[68]. The Ag(100), Cu(100), and Rh(100) surfaces bind

H most stably on the hollow sites at low coverage, but at high coverage the p4g structure (Figure

3f) is most stable for Ag(100) and Cu(100), while the 2/3 hol + 1/3 bri structure (Figure 3e) is most

stable for Rh(100). X-ray photoelectron spectroscopy studies observed similar shifts in site

preference from hollow to bridge sites upon increasing coverage for Rh(100),[69] whereas low-

energy electron-diffraction and other experimental techniques observed similar p4g

reconstructions on Cu(100) at high coverage.[39,41,42] We, however, found no reports of H-induced

reconstruction on the Ag(100) surface, which may be because H_2 does not dissociate on it.[70]

Further, we could not find experiments where pre-dissociated atomic H was dosed to Ag(100).

The TIEs for the most stable open-surface adlayer structures all decrease upon increasing coverage (Table 2 and Figure 4), like for the close-packed surfaces. On the five surfaces where the preferred H adsorption sites were unchanged, the TIEs decreased by an average of 0.12. Like the decreases seen for the close-packed surfaces, this is due to an increase in the vibrational frequencies of the metal-H bonds.[62]

The changes in the preferred adsorption sites for Ag(100), Cu(100), and Rh(100) however contributed to a large average decrease of 0.48 in their TIEs upon increasing H coverage from 0.11 to 1 ML. The reason for this is as follows: at low coverage, H binds on hollow sites on all three surfaces, giving rise to soft vibrational modes and low vibrational frequencies, and thus leading to large TIEs. At high coverage however, H binds on p4g hollow sites (Ag, Cu) and (100) bridge sites (Rh), which have much harder vibrational modes and higher vibrational frequencies, thus leading to smaller TIEs.

From the large overlaps of the high- and low-coverage TIE ranges (Figure 4), whether the TIE increases or decreases with coverage depends on how the preferred adsorption structures change as coverage increases—that is, structural changes may greatly affect TIEs. Out of the eight close-packed surfaces we studied, changes in the preferred H adsorption structures occurred for three surfaces (Ag(100), Cu(100), and Rh(100)), and the TIEs decreased with increasing coverage in all three cases. We, however, cannot preclude scenarios where changes in the preferred H adsorption structures may lead to increases in TIEs with coverage for other transition metal systems not studied in this work.

3.1.3.   Stepped Surfaces
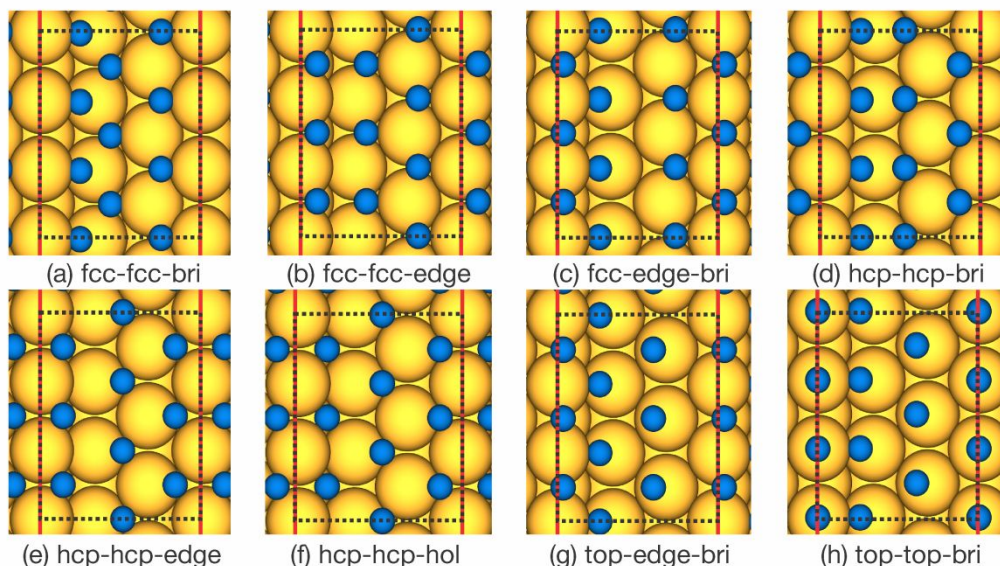
Figure 5 Top views of 1 monolayer H adlayer structures on stepped fcc (211) surfaces. See main text for explanations of structure nomenclature. Red lines indicate the step edges. The unit cell is marked by dashed lines. Color code: yellow – metal, blue – H.

Figure 5 shows the eight adlayer structures we identified for adsorption of 1 ML H on the stepped fcc (211) surfaces of Ag, Au, Cu, Ir, Ni, Pd, Pt, and Rh. These structures are labelled as triplets of site names—*i)* fcc-fcc-bri, *ii)* fcc-fcc-edge, *iii)* fcc-edge-bri, *iv)* hcp-hcp-bri, *v)* hcp-hcp-edge, *vi)* hcp-hcp-hol, *vii)* top-edge-bri, and *viii)* top-top-bri—because there are three columns of H adatoms with three symmetry-equivalent H in each column for all structures. Columns on the (111) terraces are denoted by "top", "fcc", or "hcp", if H binds on top, fcc-like, or hcp-like hollow sites respectively. Columns on the (100) steps are denoted by "hol", 'bri", and "edge", if H binds on hollow, bridge, and step edge sites respectively. An fcc-edge-bri structure thus refers to an adlayer structure with H binding on the fcc-like sites of the (111) terrace, and the step edges and bridge sites of the (100) step. Although other high-symmetry structures were observed during our studies, they were energetically less favorable (> 0.2 eV) than the ones we considered. Low-coverage structures involve single H atoms binding at various high-symmetry site types on the (211) surface, illustrations of which are shown in Figure S1e.

22

Table 3 displays the relevant thermodynamic properties and TIEs for H_2/D_2 dissociative adsorption associated with these structures. For each metal, table entries are ordered by stability; those which are most stable, having the largest absolute $\overline{BE} + \overline{ZPE_H}$, come first. Vibrational frequencies of the high- and low-coverage structures can be found in Table S3.

Table 3 Calculated thermodynamic properties for H/D adsorption at 623 K and 0.1 atm H_2/D_2 pressure on stepped surfaces, arranged in alphabetical order. Properties include average binding energies ($\overline{BE}$, eV), average zero-point energy corrected binding energies ($\overline{BE} + \overline{ZPE}$, eV), average zero-point energies ($\overline{ZPE}$, eV), and ZPE (TIE$_{ZPE}$) and entropic contributions (TIE$_{Entropy}$) to the overall thermodynamic isotope effect (TIE). See Methods for the definitions of these terms. For each surface and coverage, only stable structures are shown, and the entries are ordered by $\overline{BE} + ZPE_H$, with the most stable states first.

Surface	Coverage / ML	Structure	Average BEs / eV			Average ZPEs /		TIE Values		
			$\overline{BE}$	$\overline{BE} + ZPE_H$	$\overline{BE} + ZPE_D$	ZPE_H	ZPE_D	TIE$_{ZPE}$	TIE$_{Entropy}$	TIE
Ag(211)	0.11	hcp_a1	-2.13	-1.99	-2.03	0.138	0.097	0.96	0.99	0.95
		fcc_c2	-2.07	-1.93	-1.97	0.138	0.098	0.95	0.99	0.94
		hcp_c1	-2.06	-1.92	-1.96	0.145	0.103	0.88	1.02	0.90
		fcc_b2	-2.02	-1.88	-1.92	0.143	0.101	0.90	1.01	0.91
		top_b	-1.88	-1.75	-1.79	0.138	0.097	0.96	1.06	1.01
	1.00	hcp-hcp-hol	-2.00	-1.86	-1.90	0.141	0.100	0.92	1.02	0.94
		fcc-fcc-edge	-1.98	-1.81	-1.86	0.165	0.116	0.71	1.13	0.81
		hcp-hcp-bri	-1.95	-1.79	-1.84	0.161	0.114	0.74	1.22	0.90
		fcc-fcc-bri	-1.93	-1.77	-1.82	0.160	0.113	0.75	1.12	0.84
		fcc-edge-bri	-1.91	-1.75	-1.80	0.163	0.115	0.73	1.13	0.82
Au(211)	0.11	bri_a	-2.29	-2.14	-2.18	0.157	0.111	0.77	1.12	0.87
		fcc_c2	-2.12	-1.99	-2.03	0.132	0.093	1.02	0.97	0.99
		top_b	-2.11	-1.95	-1.99	0.160	0.113	0.75	1.13	0.85
		hcp_c1	-2.06	-1.92	-1.96	0.137	0.097	0.96	0.99	0.95
		fcc_b2	-2.02	-1.88	-1.92	0.142	0.100	0.91	1.01	0.92
		top_a	-2.02	-1.87	-1.91	0.153	0.108	0.81	1.16	0.95
		top_c	-1.86	-1.71	-1.76	0.149	0.105	0.85	1.15	0.98
	1.00	fcc-edge-bri	-2.10	-1.93	-1.98	0.162	0.115	0.73	1.12	0.82
		fcc-fcc-edge	-2.05	-1.90	-1.94	0.152	0.108	0.82	1.08	0.88
		fcc-fcc-bri	-1.98	-1.82	-1.87	0.160	0.113	0.75	1.12	0.84
Cu(211)	0.11	hcp_a1	-2.55	-2.39	-2.43	0.166	0.118	0.70	1.13	0.79
		fcc_c2	-2.47	-2.30	-2.35	0.167	0.118	0.69	1.13	0.78
		hcp_c1	-2.43	-2.26	-2.31	0.173	0.122	0.65	1.16	0.76
		fcc_b2	-2.38	-2.21	-2.26	0.169	0.119	0.68	1.14	0.78
		hol	-2.30	-2.19	-2.22	0.109	0.077	1.31	0.89	1.16
		top_b	-2.20	-2.05	-2.09	0.152	0.107	0.82	1.14	0.94
	1.00	hcp-hcp-hol	-2.35	-2.18	-2.23	0.169	0.120	0.68	1.15	0.78
		fcc-fcc-edge	-2.32	-2.13	-2.19	0.191	0.135	0.54	1.28	0.69

24

		hcp-hcp-bri	-2.28	-2.09	-2.15	0.188	0.133	0.55	1.26	0.70
		fcc-edge-bri	-2.23	-2.04	-2.09	0.185	0.131	0.57	1.25	0.71
		fcc-fcc-bri	-2.20	-2.00	-2.06	0.198	0.140	0.50	1.32	0.66
Ir(211)	0.11	bri_a	-3.06	-2.89	-2.94	0.173	0.122	0.65	1.19	0.78
		top_a	-2.90	-2.73	-2.78	0.167	0.118	0.70	1.21	0.84
		top_b	-2.87	-2.70	-2.75	0.170	0.120	0.67	1.17	0.79
		top_c	-2.66	-2.47	-2.53	0.186	0.132	0.56	1.27	0.72
		hcp_c1	-2.57	-2.44	-2.48	0.130	0.092	1.04	1.01	1.05
		bri_bc	-2.58	-2.43	-2.48	0.149	0.105	0.85	1.09	0.92
		fcc_c2	-2.57	-2.43	-2.47	0.138	0.097	0.96	1.01	0.97
		fcc_b2	-2.55	-2.41	-2.45	0.142	0.100	0.92	1.03	0.94
	1.00	fcc-edge-bri	-2.81	-2.63	-2.68	0.177	0.125	0.62	1.20	0.75
		top-edge-bri	-2.82	-2.63	-2.68	0.186	0.131	0.57	1.25	0.71
		top-top-bri	-2.75	-2.56	-2.62	0.184	0.130	0.58	1.25	0.72
		fcc-fcc-edge	-2.69	-2.53	-2.58	0.157	0.111	0.78	1.10	0.86
		hcp-hcp-edge	-2.67	-2.51	-2.56	0.151	0.107	0.83	1.08	0.89
Ni(211)	0.11	hcp_a1	-2.84	-2.67	-2.72	0.174	0.123	0.65	1.17	0.76
		fcc_c2	-2.78	-2.60	-2.66	0.174	0.123	0.64	1.17	0.75
		hcp_c1	-2.77	-2.59	-2.65	0.178	0.126	0.61	1.19	0.73
		bri_a	-2.76	-2.59	-2.64	0.165	0.117	0.71	1.22	0.86
		hol	-2.68	-2.57	-2.61	0.112	0.079	1.27	0.90	1.14
		fcc_b2	-2.74	-2.57	-2.62	0.174	0.123	0.64	1.17	0.75
		top_b	-2.61	-2.44	-2.49	0.161	0.114	0.74	1.18	0.87
	1.00	hcp-hcp-hol	-2.77	-2.59	-2.64	0.181	0.128	0.60	1.21	0.73
		fcc-fcc-edge	-2.73	-2.54	-2.59	0.191	0.135	0.53	1.28	0.68
		fcc-edge-bri	-2.67	-2.48	-2.53	0.189	0.134	0.53	1.29	0.69
Pd(211)	0.11	hcp_c1	-2.81	-2.64	-2.69	0.163	0.115	0.72	1.11	0.80
		fcc_b2	-2.81	-2.64	-2.69	0.164	0.116	0.72	1.11	0.80
		hcp_a1	-2.80	-2.64	-2.68	0.161	0.114	0.74	1.10	0.82
		fcc_c2	-2.79	-2.63	-2.68	0.161	0.114	0.74	1.10	0.81
		bri_a	-2.76	-2.59	-2.64	0.169	0.120	0.68	1.21	0.82
		top_b	-2.66	-2.50	-2.55	0.163	0.116	0.72	1.18	0.85
	1.00	hcp-hcp-hol	-2.73	-2.59	-2.63	0.145	0.103	0.88	1.04	0.91
		fcc-fcc-edge	-2.73	-2.56	-2.61	0.170	0.120	0.67	1.16	0.78
		fcc-edge-bri	-2.68	-2.51	-2.56	0.175	0.123	0.64	1.19	0.76
		fcc-fcc-bri	-2.66	-2.48	-2.53	0.180	0.127	0.60	1.21	0.73

Pt(211)	0.11	bri_a	-2.90	-2.73	-2.78	0.170	0.120	0.67	1.18	0.80
		top_a	-2.75	-2.58	-2.63	0.176	0.124	0.63	1.24	0.78
		top_b	-2.74	-2.57	-2.62	0.173	0.122	0.65	1.20	0.78
		top_c	-2.72	-2.53	-2.58	0.188	0.133	0.55	1.28	0.70
		fcc_c2	-2.66	-2.53	-2.57	0.135	0.095	0.99	0.99	0.98
		bri_ca	-2.66	-2.52	-2.56	0.149	0.106	0.84	1.10	0.93
		hcp_c1	-2.63	-2.49	-2.53	0.134	0.095	0.99	1.00	0.99
		fcc_b2	-2.62	-2.47	-2.52	0.142	0.100	0.91	1.03	0.94
		bri_bc	-2.63	-2.47	-2.52	0.162	0.114	0.74	1.15	0.85
	1.00	fcc-edge-bri	-2.77	-2.60	-2.65	0.172	0.122	0.66	1.17	0.77
		top-edge-bri	-2.75	-2.57	-2.62	0.182	0.129	0.59	1.24	0.73
		fcc-fcc-edge	-2.71	-2.55	-2.60	0.156	0.110	0.78	1.09	0.86
		top-top-bri	-2.70	-2.52	-2.57	0.185	0.131	0.57	1.26	0.72
		fcc-fcc-bri	-2.59	-2.43	-2.48	0.167	0.118	0.70	1.15	0.80
Rh(211)	0.11	bri_a	-2.85	-2.69	-2.73	0.167	0.118	0.69	1.18	0.82
		hcp_a1	-2.81	-2.65	-2.70	0.154	0.109	0.80	1.08	0.87
		hcp_c1	-2.75	-2.59	-2.64	0.158	0.112	0.77	1.09	0.84
		top_b	-2.75	-2.59	-2.64	0.161	0.114	0.74	1.15	0.85
		fcc_b2	-2.74	-2.58	-2.62	0.158	0.112	0.77	1.09	0.83
		fcc_c2	-2.73	-2.57	-2.61	0.158	0.112	0.76	1.09	0.83
	1.00	fcc-edge-bri	-2.76	-2.58	-2.63	0.177	0.125	0.63	1.20	0.75
		hcp-hcp-edge	-2.74	-2.57	-2.62	0.166	0.118	0.70	1.14	0.80
		fcc-fcc-edge	-2.74	-2.57	-2.62	0.168	0.119	0.69	1.15	0.79
		hcp-hcp-bri	-2.68	-2.51	-2.56	0.165	0.117	0.71	1.14	0.81
		fcc-fcc-bri	-2.63	-2.46	-2.51	0.176	0.124	0.63	1.19	0.75
		top-edge-bri	-2.61	-2.44	-2.49	0.167	0.118	0.69	1.19	0.82
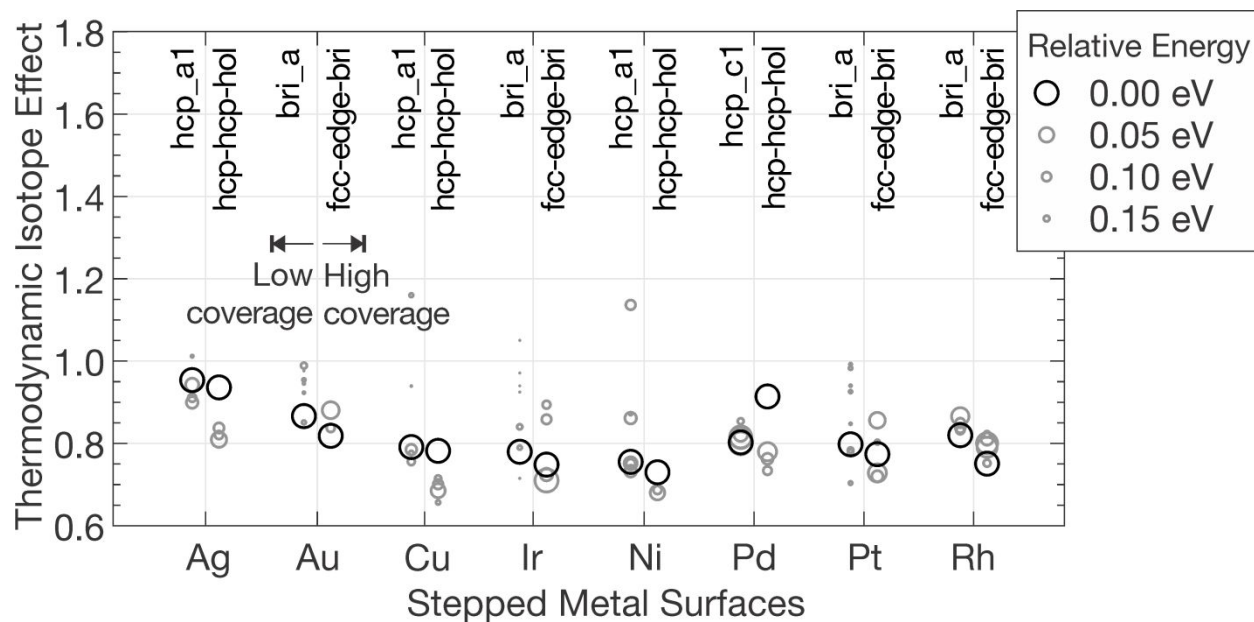
Figure 6 Calculated thermodynamic isotope effects (TIEs) for H_2/D_2 dissociative adsorption on stepped surfaces. Circles mark the TIE for each calculated structure in Table 3. For each metal, the left-most data points correspond to the low coverage (1/9 ML) TIEs; the right-most data points correspond to the high coverage (1 ML) TIEs. Larger circles reflect more stable structures; the circles sizes are based on a Boltzmann distribution at 623 K. The most stable structures for each surface and coverage are highlighted in black and are labelled by their names at the top *x*-axis. All TIEs are evaluated at 623 K and 0.1 atm H_2/D_2 pressure.

For the stepped surfaces, increasing coverage necessarily leads to changes in the preferred adsorption sites of H—at low coverage, H occupies a single adsorption site type; at high coverage however, H is forced to occupy a mixture of different adsorption site types due to the low symmetry of the (211) surface (Figure 6 and Table 3). These changes in the TIE are partially attributable to the occupation of multiple binding site types with increasing coverage. This however cannot be the sole reason; if it were, we would expect the TIEs of the high-coverage structures to be simple linear combinations of the TIEs of the low-coverage structures. This hypothesis fails on a simple test: the smallest TIEs of the high-coverage structures are less than the smallest TIEs of the low-coverage structures, except for Pt(211) (Figure 6).

The decrease in TIEs must thus be a combined effect of both higher vibrational frequencies and changes in preferred adsorption sites, where the former exerts a persistent, predictable dampening influence on the TIE. This is consistent with high-coverage structures possessing larger average ZPEs those of the low-coverage structures. Often, the combination of the two effects decreases the TIE. In the case of Pd(211) however, the changes in preferred adsorption sites exert a larger opposite influence, leading to an overall increase in the TIEs.

3.2. Kinetic Isotope Effects of H_2/D_2 Dissociative Adsorption
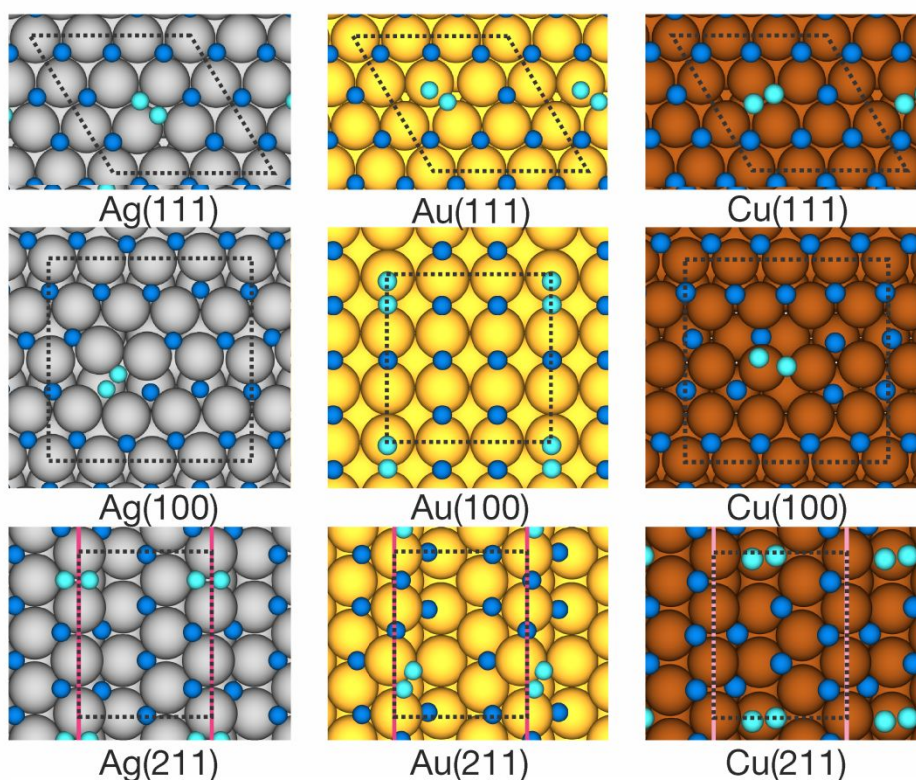
Figure 7 Top views of most stable high-coverage transition state structures for H_2/D_2 dissociative adsorption on the fcc (111), fcc (100), and fcc (211) surfaces of Ag, Au, and Cu. Pink lines mark the step edges of the (211) surfaces. The unit cell is marked by dashed lines. Color code: grey – Ag, yellow – Au, brown – Cu, blue – spectator H, cyan – dissociating H_2 molecule.

To complement our analysis of the TIEs of H_2/D_2 dissociative adsorption, we additionally calculated KIEs for the (111), (100), and (211) surfaces of the three noble metals, Au, Ag, and Cu, chosen because H_2/D_2 dissociative adsorption is highly activated on their surfaces.[71–75]

Figure 7 shows the structures of the most stable high-coverage transition states we identified; those of the less stable transition states are shown in Figures S4-6 for Ag, Au, and Cu respectively. The most stable low-coverage transition states, obtained from our previous work,[31] are shown in Figure S7. Table 4 displays kinetic properties and KIEs, evaluated at 623 K and 0.1 atm H_2/D_2 pressure, associated with these transition states. Table entries are ordered by stability; those which are most stable, having the largest absolute average $\overline{BE} + \overline{ZPE_H}$, come first. Vibrational frequencies of the high- and low-coverage structures can be found in Table S4.

Table 4 Calculated kinetic properties for H_2/D_2 dissociative adsorption at 623 K and 0.1 atm H_2/D_2 pressure on Au, Ag, and Cu surfaces. Properties include activation energy barriers (E_a, eV), zero-point energy corrected activation barriers ($E_a+\Delta ZPE$, eV); average binding energies ($\overline{BE}$, eV), average zero-point-energy-corrected binding energies ($\overline{BE} + \overline{ZPE}$, eV), and average zero-point energies ($\overline{ZPE}$, eV) for the transition states; and ZPE (KIE_{ZPE}) and entropic contributions ($KIE_{Entropy}$) to the overall kinetic isotope effect (KIE). See Methods for the definitions of these terms. For each surface and coverage, the entries are ordered by $\overline{BE} + \overline{ZPE}_H$, with the most stable states first. Entry numbers differentiate between the different transition state structures, listed in Figures S4-6 in the Supporting Information. Listed coverage indicates the coverage at the final state of the dissociation event.

Surface	Coverage / ML	Entry No.	Activation Energies / eV			Average BEs / eV			Average ZPEs / eV		KIE Values		
			E_a	$E_a+\Delta ZPE_H$	$E_a+\Delta ZPE_D$	$\overline{BE}$	$\overline{BE} + \overline{ZPE}_H$	$\overline{BE} + \overline{ZPE}_D$	$\overline{ZPE}_H$	$\overline{ZPE}_D$	KIE_{ZPE}	$KIE_{Entropy}$	KIE
Ag(111)	0.22	1	1.09	1.03	1.05	-1.73	-1.63	-1.66	0.102	0.072	1.41	1.27	1.79
	1.00	1	1.48	1.47	1.47	-1.97	-1.82	-1.86	0.156	0.110	1.07	1.43	1.53
		2	1.47	1.45	1.46	-1.97	-1.81	-1.86	0.155	0.109	1.07	1.42	1.53
Au(111)	0.22	1	0.97	0.95	0.95	-1.79	-1.67	-1.71	0.124	0.088	1.11	1.43	1.59
	1.00	1	1.42	1.43	1.43	-1.95	-1.81	-1.85	0.143	0.101	0.94	1.51	1.43
		2	1.42	1.43	1.43	-1.93	-1.79	-1.83	0.142	0.100	0.92	1.53	1.41
Cu(111)	0.22	1	0.48	0.47	0.48	-2.03	-1.91	-1.94	0.128	0.090	1.07	1.45	1.55
	1.00	1	0.89	0.91	0.90	-2.31	-2.13	-2.18	0.182	0.128	0.88	1.54	1.35
		2	0.88	0.91	0.90	-2.31	-2.13	-2.18	0.181	0.128	0.87	1.55	1.34
Ag(100)	0.22	1	1.10	1.06	1.07	-1.73	-1.61	-1.65	0.115	0.082	1.22	1.33	1.62
	1.00	1	0.91	1.00	0.97	-2.00	-1.86	-1.90	0.144	0.102	0.62	1.71	1.06
		2	1.13	1.16	1.15	-1.99	-1.85	-1.89	0.142	0.100	0.86	1.53	1.32
		3	1.42	1.46	1.45	-1.97	-1.83	-1.87	0.142	0.100	0.81	1.63	1.31
		4	1.63	1.66	1.65	-1.96	-1.82	-1.86	0.143	0.101	0.87	1.54	1.33
Au(100)	0.22	1	0.69	0.68	0.68	-1.93	-1.80	-1.84	0.129	0.092	1.05	1.46	1.53
	1.00	1	0.87	0.88	0.88	-2.11	-1.95	-2.00	0.158	0.112	0.95	1.51	1.43
		2	0.97	0.93	0.95	-2.09	-1.94	-1.98	0.153	0.108	1.25	1.33	1.66
Cu(100)	0.22	1	0.56	0.54	0.55	-2.00	-1.87	-1.91	0.126	0.089	1.09	1.41	1.53
	1.00	1	0.78	0.84	0.82	-2.32	-2.16	-2.21	0.165	0.116	0.71	1.70	1.21
		2	0.75	0.78	0.78	-2.31	-2.15	-2.20	0.160	0.113	0.84	1.57	1.31
		3	0.88	0.94	0.92	-2.30	-2.14	-2.19	0.161	0.114	0.71	1.72	1.23

Ag(211)	0.22	1	1.10	1.04	1.06	-1.72	-1.62	-1.65	0.101	0.071	1.43	1.26	1.80
	1.00	1	1.26	1.24	1.25	-1.94	-1.80	-1.84	0.139	0.098	1.07	1.45	1.55
		2	1.50	1.49	1.49	-1.94	-1.80	-1.84	0.142	0.100	1.01	1.46	1.47
		3	1.67	1.64	1.65	-1.94	-1.80	-1.84	0.144	0.102	1.22	1.37	1.67
		4	1.57	1.58	1.58	-1.94	-1.79	-1.84	0.148	0.104	0.92	1.60	1.46
		5	1.11	1.06	1.08	-1.93	-1.78	-1.83	0.150	0.106	1.29	1.33	1.71
		6	1.14	1.18	1.17	-1.93	-1.78	-1.82	0.160	0.113	0.78	1.65	1.28
		7	1.45	1.43	1.44	-1.90	-1.77	-1.81	0.129	0.091	1.11	1.41	1.56
		8	1.25	1.28	1.27	-1.93	-1.77	-1.82	0.157	0.111	0.88	1.54	1.35
		9	1.60	1.59	1.59	-1.92	-1.77	-1.82	0.155	0.110	1.05	1.44	1.51
		10	1.56	1.53	1.54	-1.91	-1.77	-1.81	0.146	0.103	1.19	1.36	1.63
		11	1.66	1.66	1.66	-1.91	-1.76	-1.81	0.147	0.104	0.97	1.49	1.45
		12	1.90	1.80	1.83	-1.89	-1.76	-1.80	0.129	0.091	1.74	1.19	2.06
		13	1.50	1.59	1.56	-1.89	-1.73	-1.78	0.156	0.110	0.63	1.73	1.09
		14	1.19	1.17	1.17	-1.88	-1.73	-1.77	0.150	0.106	1.12	1.39	1.56
		15	1.79	1.74	1.76	-1.86	-1.71	-1.75	0.151	0.107	1.33	1.32	1.76
		16	1.77	1.77	1.77	-1.86	-1.70	-1.75	0.157	0.111	1.00	1.48	1.48
Au(211)	0.22	1	0.71	0.75	0.74	-1.92	-1.77	-1.81	0.155	0.110	0.79	1.66	1.31
	1.00	1	0.80	0.85	0.83	-2.06	-1.90	-1.95	0.159	0.113	0.74	1.64	1.22
		2	1.03	1.01	1.02	-2.05	-1.89	-1.94	0.154	0.109	1.07	1.42	1.52
		3	0.93	0.93	0.93	-2.05	-1.89	-1.94	0.157	0.111	0.95	1.49	1.42
		4	1.02	1.01	1.01	-2.03	-1.87	-1.92	0.155	0.110	1.03	1.46	1.51
		5	1.09	1.10	1.10	-2.02	-1.86	-1.91	0.157	0.111	0.98	1.51	1.48
		6	1.28	1.27	1.28	-2.00	-1.86	-1.90	0.149	0.105	1.02	1.49	1.52
		7	0.65	0.65	0.65	-1.98	-1.84	-1.88	0.145	0.102	0.97	1.54	1.49
		8	1.10	1.06	1.08	-1.97	-1.83	-1.87	0.141	0.100	1.22	1.36	1.66
Cu(211)	0.22	1	0.43	0.45	0.45	-2.06	-1.91	-1.96	0.146	0.103	0.88	1.58	1.39
	1.00	1	0.77	0.80	0.79	-2.29	-2.13	-2.18	0.164	0.116	0.85	1.53	1.31
		2	0.61	0.62	0.62	-2.29	-2.13	-2.18	0.164	0.116	0.98	1.50	1.47
		3	0.99	1.01	1.01	-2.28	-2.11	-2.16	0.164	0.116	0.88	1.54	1.35
		4	1.07	1.11	1.10	-2.28	-2.11	-2.16	0.173	0.123	0.83	1.60	1.33
		5	1.21	1.14	1.16	-2.27	-2.11	-2.16	0.161	0.114	1.49	1.23	1.84

6	0.83	0.87	0.86	-2.26	-2.10	-2.15	0.155	0.110	0.81	1.67	1.35
7	0.43	0.44	0.44	-2.28	-2.10	-2.15	0.177	0.125	0.93	1.51	1.41
8	0.68	0.72	0.71	-2.26	-2.08	-2.13	0.180	0.127	0.76	1.64	1.25
9	0.61	0.73	0.70	-2.26	-2.08	-2.13	0.176	0.125	0.52	1.91	1.00
10	1.04	1.06	1.05	-2.25	-2.08	-2.13	0.177	0.125	0.90	1.55	1.39
11	0.72	0.77	0.76	-2.25	-2.07	-2.13	0.180	0.127	0.77	1.69	1.29
12	0.91	0.93	0.92	-2.25	-2.07	-2.12	0.176	0.124	0.89	1.51	1.35
13	1.12	1.21	1.18	-2.24	-2.07	-2.12	0.174	0.123	0.61	1.84	1.13
14	1.10	1.23	1.19	-2.20	-2.02	-2.08	0.177	0.125	0.50	1.93	0.97
15	1.08	1.13	1.11	-2.18	-2.00	-2.05	0.177	0.125	0.77	1.62	1.24
16	1.83	1.90	1.88	-2.16	-1.99	-2.04	0.172	0.122	0.68	1.77	1.21
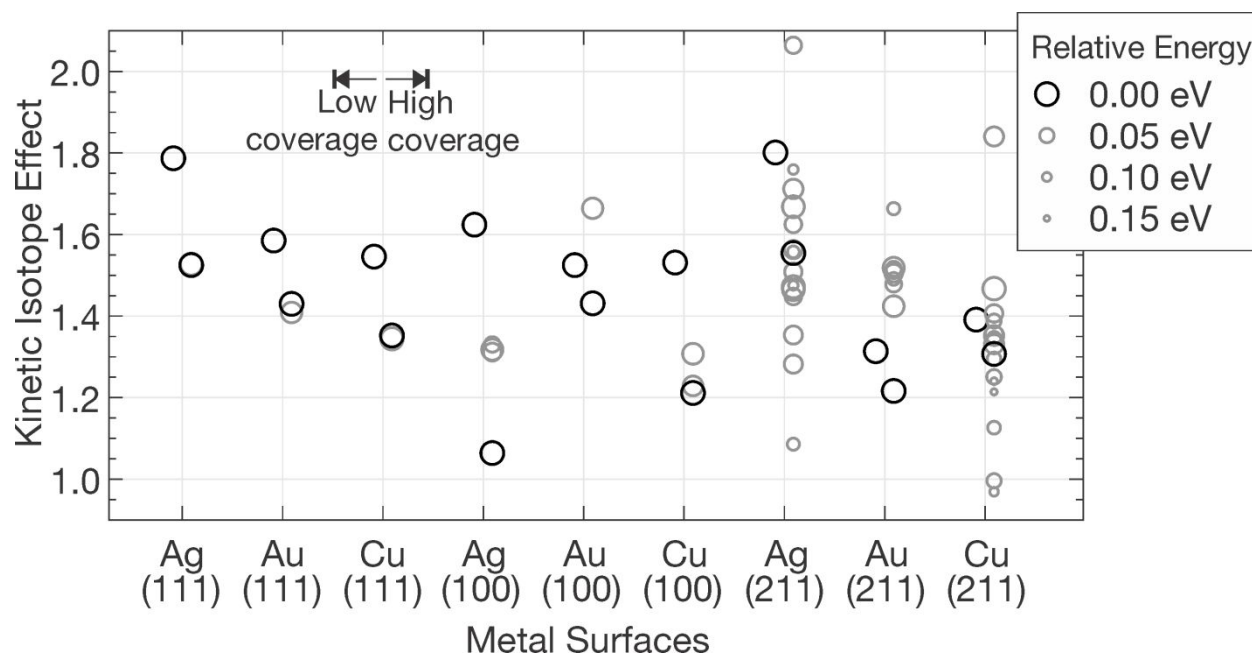
Figure 8 Calculated kinetic isotope effects (KIEs) for H_2/D_2 dissociative adsorption on Ag, Au, and Cu surfaces. For each metal, the left-most data point corresponds to the low coverage (2/9 ML) KIE; the right-most data point corresponds to the high coverage (1 ML) KIE. Circles mark the KIE for each calculated structure in Table 4. Larger circles reflect more stable structures; the circles sizes are based on a Boltzmann distribution at 623 K. The most stable structures for each surface and coverage are highlighted in black and correspond to entry numbers of 1 for each surface and coverage in Table 4. All KIEs are evaluated at 623 K and 0.1 atm H_2/D_2 pressure.

The KIEs of the most stable high coverage transition states are all lower than those of the most stable low coverage ones (Table 4 and Figure 8). By visual inspection (Figure 7 versus Figure S7), only the (111) surfaces and Au(100) retained similar most stable transition state structures upon going to higher coverages. On these surfaces, the KIEs decreased by an average of 0.18, with Au(111) showing the largest decrease of 0.26. The reasons driving this decrease in the KIEs are similar to those driving the decreases in the TIEs: increases in the vibrational frequencies of the transition states, as implied by the increase in their average ZPEs, which lead to greater destabilization of the H-transition state relative to the D-transition state.

The remaining surfaces have different high- and low-coverage transition state geometries; surface reconstructions were also observed for Ag(100) and Cu(100). For these surfaces, the TIEs decreased by an average of 0.26, with Ag(100) showing the largest decrease of 0.56. The decrease

33

in KIEs for some of these surfaces however seems quite fortuitous. On Au(211) for example, all higher coverage transition state structures except the most stable one give rise to larger KIEs than that of the low coverage transition state structure. Additionally, many structures are only slightly less stable—with two structures just 0.01 eV per H higher in energy—than the most stable structure. These examples of structures which are very close in energy, and yet have very different KIEs, emphasize the unpredictability of the influence of changes in the preferred adsorption sites on isotope effects.

3.3. Temperature Dependences of Thermodynamic and Kinetic Isotope Effects
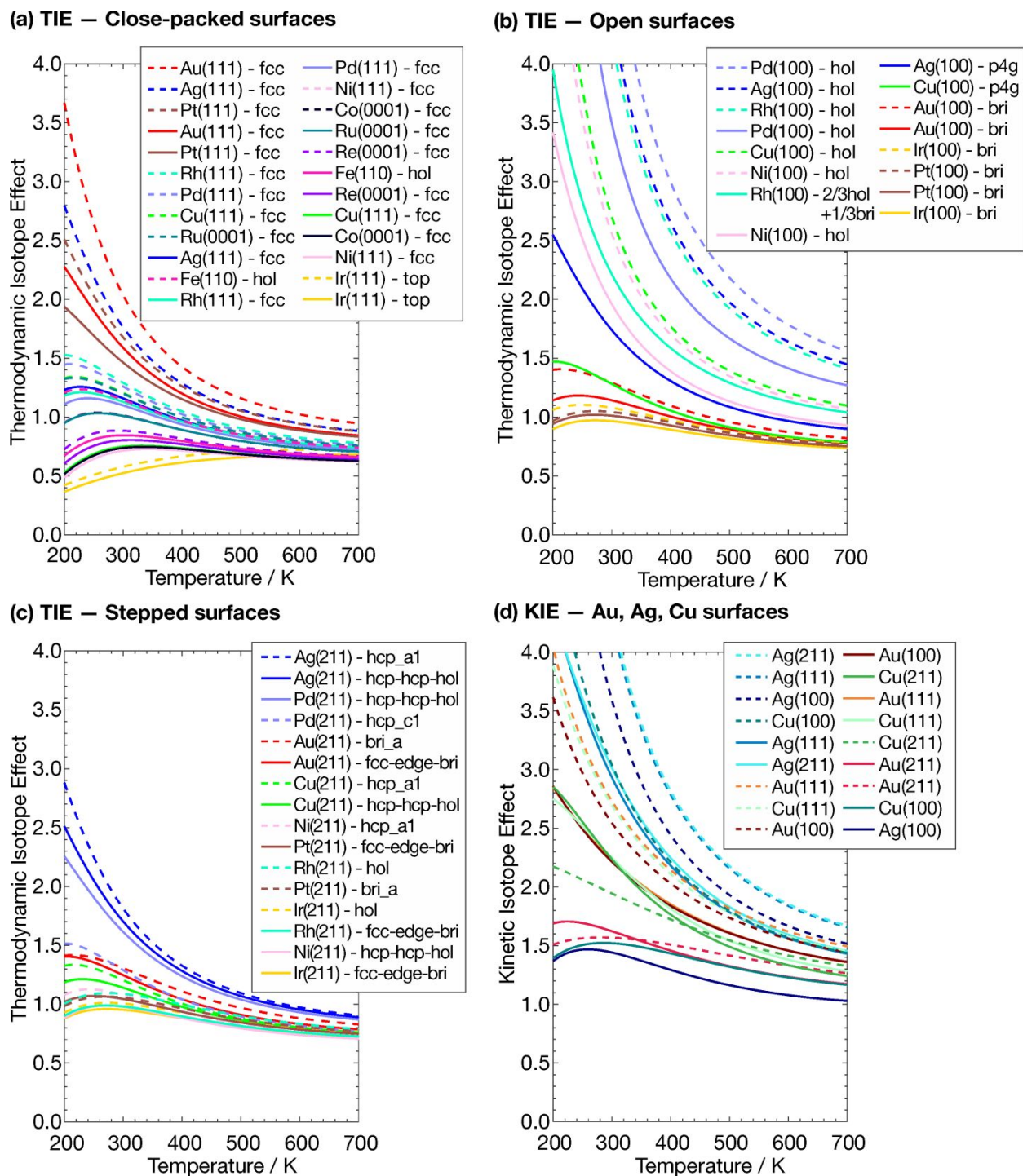
Figure 9 Temperature dependence of (a-c) thermodynamic isotope effects (TIEs) for the most stable adsorption structures on (a) close-packed, (b) open, and (c) stepped transition metal surfaces; and (d) kinetic isotope effects (KIEs) on close-packed, open, and stepped surfaces of Ag, Au, and Cu. Dashed and full lines represent low coverage and high coverage structures respectively.

All calculated TIE and KIE values until here were evaluated at a temperature of 623 K and a H_2/D_2

pressure of 0.1 atm. We find that pressure does not affect our calculated values; although the

translational entropy of $H_2(g)$ and $D_2(g)$ depends on pressure, it changes equally with pressure for

both species. Changes in temperature however affect the entropies of gas-phase H_2, adsorbed

species, and transition states unequally, and thus may alter our calculated TIEs and KIEs. Note

that changes in temperature and pressure can also affect the coverage of H—for example,

increasing temperature and decreasing pressure will reduce the coverage of H—which we do not

consider in our analysis.

We plot in Figure 9a-c TIEs evaluated between 200 – 700 K; and in Figure 9d KIEs evaluated in

the same temperature range. Only the most stable structures at high (Figure 9; full lines) and low

(Figure 9; dashed lines) coverage were considered. Similar plots for the TIEs of less stable

structures are in Figures S8-10 for the close-packed, open, and stepped surfaces respectively; and

similar plots for the KIEs for less stable transition states are in Figure S11.

Importantly, we find that the differences in isotope effects between different structures narrow

with increasing temperature. For example, at 200 K, the TIEs for the low (Figure 9a; red dashed

line) and high (Figure 9a; red full line) coverage structures of Au(111) are 3.67 and 2.27

respectively, differing by 1.40. At 700 K however, this difference narrows to just 0.11, with TIEs

of 0.95 and 0.84 for the high- and low-coverage structures respectively. This is because the TIEs

for all surfaces tend to a constant value of ~1 at high temperatures. A similar effect is observed for

the KIEs, which tend to ~1.5. For a detailed explanation of this phenomenon, see Section S3.

Trends in isotope effects across the different structures and surfaces are relatively unchanged with

changing temperature, as evidenced by the scarcity of line crossings in Figure 9. In the rare event

of a change in the trends, the isotope effects remain close to each other. For example, the lines representing the KIEs of the high- and low-coverage transition states of Au(211) (Figure 9d; red lines) cross but stay within 0.2 of each other throughout the temperature range.

Overall, higher temperatures diminish the changes in isotope effects induced by increasing coverage. The sign of these changes is however rarely affected. Thus, for most surfaces, higher temperatures reduce the magnitude of the decrease in isotope effects caused by increasing coverage.

4.　　Discussion

4.1.　　Implications of Findings

Table 5 Summary of changes in thermodynamic and kinetic isotope effects (TIEs and KIEs) upon increasing coverage, from 0.11 to 1.00 ML H for the TIEs and from 0.22 ML to 1.00 ML H for the KIEs. All identified high-coverage structures were included, and changes were evaluated with respect to the most stable low-coverage structures for each metal and facet. Isotope effects are evaluated at 623 K and 0.1 atm H_2/D_2 pressure.

	Thermodynamic Isotope Effect			Kinetic Isotope Effect			Overall
	Close-packed	Open	Stepped	Close-packed	Open	Stepped	
Average Change	−0.05	−0.41	−0.04	−0.21	−0.25	−0.11	−0.14
Number of Structures with Increased Isotope Effects	4	1	7	0	1	11	24
Number of Structures with Decreased Isotope Effects	23	21	28	6	8	29	115

Our results reveal two ways in which increasing coverage can influence isotope effects: increases in the vibrational frequencies of adsorbed H, and changes to the preferred H adsorption sites. Whereas the former always leads to smaller isotope effects, the latter can lead to either smaller or larger isotope effects.

37

Empirically, our findings show that increasing H coverage results in smaller kinetic and thermodynamic isotope effects (KIEs and TIEs) in most cases. After considering *all* high-coverage structures we identified, and comparing them to their corresponding most stable low-coverage structures, only 24 showed increases in their isotope effects with increasing coverage, while 115 showed decreases (Table 5). The average change is also negative: –0.14. These are by no means comprehensive statistics. They however indicate that the inevitable increases in the H vibrational frequencies with increasing coverage, regardless of changes in the preferred adsorption sites, exert a strong dampening influence on the isotope effects.

If we could somehow predict that the preferred adsorption site would not change with increasing coverage, then we could be almost certain that the isotope effects would decrease with increasing coverage. Besides costly first-principles calculations, descriptors such as the orbitalwise coordination number[76] may serve as approximate predictors of whether changes in adsorption sites would occur or not. These descriptors can be used to estimate the energetics of adsorption at different adsorption sites in the presence of coadsorbates, and thus serve as a useful screening tools for approximately predicting which systems are likely to experience changes in adsorption sites upon increasing coverage. Pairing this descriptor-based screening of adsorption site preferences with our general rule of thumb that isotope effects decrease when there is no change in adsorption sites will allow us to predict how isotope effects change as a function of coverage for a range of systems.

Our conclusions stand across a range of temperatures, which we show affects the magnitude of the changes in isotope effects with coverage but does not flip the sign of these changes. Higher temperatures tend to homogenize the isotope effects on different surfaces, thus leading to smaller differences in the isotope effects on surfaces with different coverage. This, however, neglects the

changes in adsorbate coverages that these temperature changes would bring about, which would have to be factored in separately.

Our results agree with the scarce literature available on this topic. The dissociative sticking coefficients of D_2 are lower than those of H_2 on Ni(100)[77] and the activation energies for H_2 dissociation are lower than those for D_2 dissociation on PdAgCu alloys[78]. These observations are consistent with the normal KIEs we calculated for Au, Ag, and Cu. Additionally, Truong and Truhlar found an increase in the KIE of H_2 dissociation on Ni(100) with increasing coverage[29], which at first seems inconsistent with our findings. They however attribute the increase to quantum tunneling, which is only expected to play a role only at temperatures less than ~200 K.[48,49] Without quantum effects, they find that the KIE instead decreases with increasing coverage[29], in agreement with our findings on Au, Ag, and Cu.

Besides quantum effects, it is important to keep in mind other limitations of our study. Firstly, we use the harmonic approximation to calculate thermodynamic quantities such as zero-point energy and entropy. We expect it to hold reasonably well as most of our vibrational modes are large (> 200 cm^{-1}). Secondly, the vibrational modes of many atoms couple to form phonons; we however do not model the effects of phonon dispersion away from the Brillouin zone center, as the dispersion of the phonon modes is weak for H adlayers,[79,80] and our relatively large unit cell sizes allow us to capture the major effects of vibrational coupling.[81] Lastly, we have focused on two extremal coverages, 1/9 and 1 ML. It is unclear what happens at intermediate coverages, which is an interesting subject for further computational studies.

At coverages > 1 ML, which are likely relevant on small nanoparticles and nanoclusters less than ~2 nm in diameter[82,83], we predict that the trend of decreasing isotope effects with increasing H

coverage should continue for most metal surfaces. Firstly, although most metals prefer to bind H at hollow sites at coverages of 1 ML or less, the occupation of bridge and top sites, which have steeper potential energy wells than hollow sites, becomes inevitable at coverages > 1 ML. This was shown on Ru(0001)[84] and Pt(111)[85] for example. Secondly, destabilizing interactions between adsorbed H increase sharply for coverages > 1 ML.[17,83–85] Both these factors likely lead to an increase in the average H vibrational frequencies and thus a decrease in the observed isotope effects.

Ni and Pd are, however, possible exceptions to these projected trends. For Ni and Pd, H prefers to occupy bulk and subsurface sites instead of further saturating the surface at coverages > 1 ML.[86,87] The impact of this on the isotope effects is unclear as the H vibrational frequencies can differ greatly depending on the type of subsurface sites occupied.[88] Further, the occupation of subsurface sites would not destabilize surface H as much as the occupation of additional surface sites would. For these metals, system-specific calculations would be needed for elucidating how subsurface sites affect the isotope effects for H_2 dissociation.

4.2. Catalytic Applications

To end our discussion, it is interesting to consider how our results may guide researchers in applying isotope effects to solve problems in catalysis. An application of our finding that TIEs vary with coverage is as a scale for quantifying equilibrium adsorbate coverages. Once calibrated with several TIE measurements at different coverages, this scale would be able to deduce the coverage of adsorbates on a surface based on subsequent TIE measurements. As the resolution of typical isotope effect measurements is around 0.1[5,8], this would work best on surfaces with large differences (> 0.1) in their high- and low-coverage TIEs, such as the open (100) surfaces (Table 5).
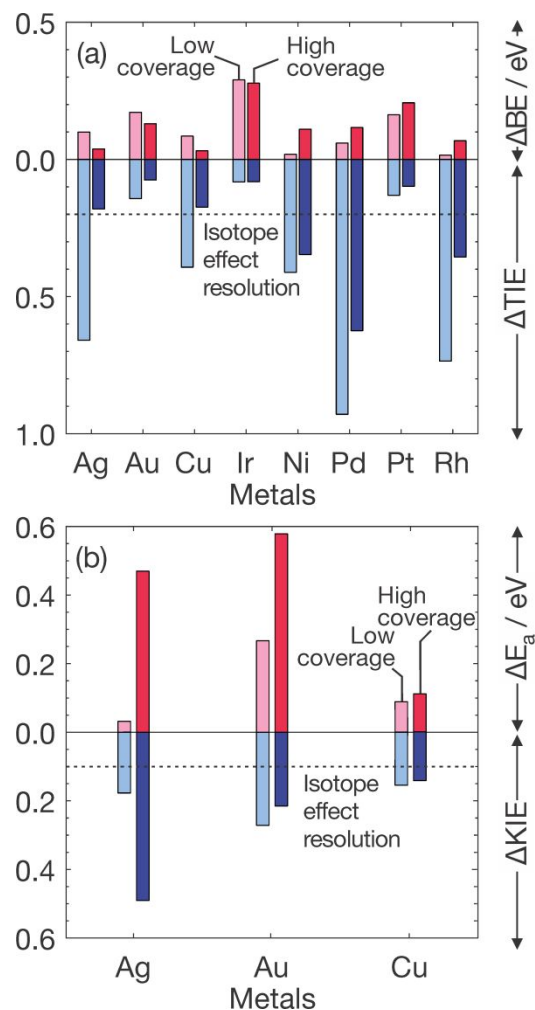
Figure 10 Structure-sensitivity of TIEs and KIEs for dissociative adsorption of H_2/D_2 on transition metal surfaces. (a) Maximum variation in TIEs (ΔTIE) and BEs (ΔBE) across the (111), (100), and (211) facets of various metals at low and high coverage. Re, Ru, Fe, and Co are not shown as only close-packed surfaces were considered for these metals. (b) Maximum variation in KIEs (ΔKIE) and activation energies (ΔE_a) across the (111), (100), and (211) facets of Ag, Au, and Cu at low and high coverage. Isotope effects are evaluated at 623 K and 0.1 atm H_2/D_2 pressure. Dashed lines mark the typical resolution of isotope effect measurements (0.1).

TIEs may also be used to elucidate the adsorption sites of H and thus the types of facets present

on nanoparticles of unknown morphology.[31] To evaluate the feasibility of this idea, we calculated

the maximum variation in average binding energies and TIEs across the various facets for each

metal we studied, at both high and low coverages. Most metals exhibit variations in the TIEs of

their facets that are larger than 0.1 (Figure 10a; light and dark blue bars), the typical resolution of isotope effect measurements.[5,8] TIEs can thus be used to distinguish between H adsorption on the different facets. This should however work better at low coverages, where the variations in TIEs are generally larger. For example, Pd exhibits a large TIE range of ~0.9 between Pd(100) and Pd(111) at low coverage (Table 1 and Table 2). At high coverage however, this difference decreases to 0.6, making it more difficult to distinguish between the two facet types. When differences in the TIEs are small however, other complementary techniques for determining adsorption site preferences may be useful. On Ir for example, the differences in the TIEs are small, but the differences in binding energies across the different facets are large (Figure 10a; pink and red bars), making calorimetry a possible alternative.

Analogous to using TIEs to determine the adsorption sites of H, KIEs may be used to identify active sites for H_2/D_2 dissociation.[31] Figure 10b shows the maximum variation in activation energies and KIEs between the facets of Ag, Au, and Cu at high and low coverage. With increasing coverage, the variations in activation energies also increase, indicating larger structure sensitivity in terms of reaction rates, whereas the differences in KIEs decrease (except for Ag), indicating smaller structure sensitivity in terms of KIEs. It is thus easier to use differences in KIEs to identify active sites at low coverages, and easier to use differences in reaction rates at high coverages.

5.   Conclusions

We elucidated the effects of coverage on the thermodynamic and kinetic isotope effects (TIEs and KIEs) of H_2/D_2 dissociative adsorption on a total of 28 different transition metal surfaces of 12 different metals. Our first-principles, density functional theory (DFT) calculations reveal that increasing coverage can influence isotope effects in two main ways. Firstly, it may change the most preferred H adsorption sites and transition state structures. This may either increase or

decrease the isotope effects. Secondly, increasing H coverage increases the vibrational frequencies of adsorbed H due to the destabilizing interactions between H species. This consistently decreases the isotope effects. For most of our studied systems, we observed an overall decrease in the isotope effects with increasing surface coverage, reflecting the more consistent nature of the latter effect. Higher temperatures reduce the magnitude of these decreases in the isotope effects.

Our work sheds light into how high coverage of adsorbates, commonly found under realistic reaction conditions, influences isotope effects. Although in this work we used atomic H as a model coadsorbate, we believe that the coverage effects we uncovered will be highly generalizable to other coadsorbates, such as hydrocarbons species that are frequently present in high coverages during hydrogenation reactions for example. This is because the fundamental mechanism by which increasing coverage influences isotope effects — via destabilizing lateral interactions between adsorbates — is independent of the adsorbate.

These insights will aid in the analysis and interpretation of experimentally measured isotope effects, and thus allow researchers to fully harness the power of isotopic substitution for elucidating mechanistic pathways. We hope that our work will also spur on further research into the multitude of potential applications of isotope effects, such as using TIEs and KIEs to elucidate the adsorption sites of H/D and active sites of H_2/D_2 dissociative adsorption.

Acknowledgements

44

References

(1)   Świderek, K.; Paneth, P. Binding Isotope Effects. *Chem. Rev.* **2013**, *113* (10), 7851–7879.

(2)   Wiberg, K. B. The Deuterium Isotope Effect. *Chem. Rev.* **1955**, *55* (4), 713–743.

(3)   Kaye, J. A. Isotope Effects in Gas-Phase Chemical Reactions and Photodissociation Processes. In *ACS Symposium Series*; American Chemical Society: Washington, DC, 1992; Vol. 502, pp 1–14.

(4)   González-Lafont, À.; Lluch, J. M. Kinetic Isotope Effects in Chemical and Biochemical Reactions: Physical Basis and Theoretical Methods of Calculation. *Wiley Interdiscip. Rev. Comput. Mol. Sci.* **2016**, *6* (5), 584–603.

(5)   Tse, E. C. M.; Hoang, T. T. H.; Varnell, J. A.; Gewirth, A. A. Observation of an Inverse Kinetic Isotope Effect in Oxygen Evolution Electrochemistry. *ACS Catal.* **2016**, *6* (9), 5706–5714.

(6)   Roca, M.; Moliner, V.; Tuñón, I. Origin of Enzymatic Kinetic Isotope Effects in Human Purine Nucleoside Phosphorylase. *ACS Catal.* **2018**, *8* (2), 815–827.

(7)   Jones, H. B. L.; Crean, R. M.; Matthews, C.; Troya, A. B.; Danson, M. J.; Bull, S. D.; Arcus, V. L.; Van Der Kamp, M. W.; Pudney, C. R. Uncovering the Relationship between the Change in Heat Capacity for Enzyme Catalysis and Vibrational Frequency through Isotope Effect Studies. *ACS Catal.* **2018**, *8* (6), 5340–5349.

(8)   Saavedra, J.; Doan, H. A.; Pursell, C. J.; Grabow, L. C.; Chandler, B. D. The Critical Role of Water at the Gold-Titania Interface in Catalytic CO Oxidation. *Science (80-.).* **2014**, *345* (6204), 1599–1602.

(9)   Izzo, J. A.; Poulsen, P. H.; Intrator, J. A.; Jørgensen, K. A.; Vetticatt, M. J. Isotope Effects Reveal an Alternative Mechanism for "Iminium-Ion" Catalysis. *J. Am. Chem. Soc.* **2018**, *140* (27), 8396–8400.

(10)   Pasquini, C.; Zaharieva, I.; González-Flores, D.; Chernev, P.; Mohammadi, M. R.; Guidoni, L.; Smith, R. D. L.; Dau, H. H/D Isotope Effects Reveal Factors Controlling Catalytic Activity in Co-Based Oxides for Water Oxidation. *J. Am. Chem. Soc.* **2019**, *141* (7), 2938–2948.

(11)   Garrett, B. C.; Truhlar, D. G. Variational Transition State Theory. Primary Kinetic Isotope Effects for Atom Transfer Reactions. *J. Am. Chem. Soc.* **1980**, *102* (8), 2559–2570.

(12)   Zhang, Y.; Karunananda, M. K.; Yu, H.-C.; Clark, K. J.; Williams, W.; Mankad, N. P.; Ess, D. H. Dynamically Bifurcating Hydride Transfer Mechanism and Origin of Inverse Isotope Effect for Heterodinuclear AgRu-Catalyzed Alkyne Semihydrogenation. *ACS Catal.* **2019**, *9* (3), 2657–2663.

(13)   Ojeda, M.; Li, A. W.; Nabar, R.; Nilekar, A. U.; Mavrikakis, M.; Iglesia, E. Kinetically Relevant Steps and H_2/D_2 Isotope Effects in Fischer-Tropsch Synthesis on Fe and Co Catalysts. *J. Phys. Chem. C* **2010**, *114* (46), 19761–19770.

(14)   Hama, T.; Ueta, H.; Kouchi, A.; Watanabe, N. Quantum Tunneling Observed without Its Characteristic Large Kinetic Isotope Effects. *Proc. Natl. Acad. Sci.* **2015**, *112* (24), 7438–7443.

(15)   Chen, K.; Iglesia, E.; Bell, A. T. Kinetic Isotopic Effects in Oxidative Dehydrogenation of Propane on Vanadium Oxide Catalysts. *J. Catal.* **2000**, *192* (1), 197–203.

(16)   Zhang, Y.; Karunananda, M. K.; Yu, H. C.; Clark, K. J.; Williams, W.; Mankad, N. P.; Ess, D. H. Dynamically Bifurcating Hydride Transfer Mechanism and Origin of Inverse Isotope Effect for Heterodinuclear AgRu-Catalyzed Alkyne Semihydrogenation. *ACS Catal.* **2019**,

9 (3), 2657–2663.

(17)   Van Helden, P.; Van Den Berg, J. A.; Weststrate, C. J. Hydrogen Adsorption on Co Surfaces: A Density Functional Theory and Temperature Programmed Desorption Study. *ACS Catal.* **2012**, *2* (6), 1097–1107.

(18)   Faglioni, F.; Goddard, W. A. Energetics of Hydrogen Coverage on Group VIII Transition Metal Surfaces and a Kinetic Model for Adsorption/Desorption. *J. Chem. Phys.* **2005**, *122* (1), 014704.

(19)   Strmcnik, D.; Tripkovic, D.; van der Vliet, D.; Stamenkovic, V.; Marković, N. M. Adsorption of Hydrogen on Pt(111) and Pt(100) Surfaces and Its Role in the HOR. *Electrochem. commun.* **2008**, *10* (10), 1602–1605.

(20)   Almithn, A.; Hibbitts, D. Effects of Catalyst Model and High Adsorbate Coverages in Ab Initio Studies of Alkane Hydrogenolysis. *ACS Catal.* **2018**, *8* (7), 6375–6387.

(21)   Lausche, A. C.; Medford, A. J.; Khan, T. S.; Xu, Y.; Bligaard, T.; Abild-Pedersen, F.; Nørskov, J. K.; Studt, F. On the Effect of Coverage-Dependent Adsorbate–Adsorbate Interactions for CO Methanation on Transition Metal Surfaces. *J. Catal.* **2013**, *307*, 275–282.

(22)   Hamada, I.; Morikawa, Y. Density-Functional Analysis of Hydrogen on Pt(111): Electric Field, Solvent, and Coverage Effects. *J. Phys. Chem. C* **2008**, *112* (29), 10889–10898.

(23)   Katsounaros, I.; Figueiredo, M. C.; Chen, X.; Calle-Vallejo, F.; Koper, M. T. M. Structure- and Coverage-Sensitive Mechanism of NO Reduction on Platinum Electrodes. *ACS Catal.* **2017**, *7* (7), 4660–4667.

(24)   Loveless, B. T.; Buda, C.; Neurock, M.; Iglesia, E. CO Chemisorption and Dissociation at High Coverages during CO Hydrogenation on Ru Catalysts. *J. Am. Chem. Soc.* **2013**, *135* (16), 6107–6121.

(25)   Liu, J.; Hibbitts, D.; Iglesia, E. Dense CO Adlayers as Enablers of CO Hydrogenation Turnovers on Ru Surfaces. *J. Am. Chem. Soc.* **2017**, *139* (34), 11789–11802.

(26)   Wu, P.; Yang, B. Significance of Surface Formate Coverage on the Reaction Kinetics of Methanol Synthesis from CO_2 Hydrogenation over Cu. *ACS Catal.* **2017**, *7* (10), 7187–7195.

(27)   Yao, Z.; Guo, C.; Mao, Y.; Hu, P. Quantitative Determination of C–C Coupling Mechanisms and Detailed Analyses on the Activity and Selectivity for Fischer–Tropsch Synthesis on Co(0001): Microkinetic Modeling with Coverage Effects. *ACS Catal.* **2019**, *9* (7), 5957–5973.

(28)   Farberow, C. A.; Dumesic, J. A.; Mavrikakis, M. Density Functional Theory Calculations and Analysis of Reaction Pathways for Reduction of Nitric Oxide by Hydrogen on Pt(111). *ACS Catal.* **2014**, *4* (10), 3307–3319.

(29)   Truong, T. N.; Truhlar, D. G. The Effects of Steps, Coupling to Substrate Vibrations, and Surface Coverage on Surface Diffusion Rates and Kinetic Isotope Effects: Hydrogen Diffusion on Ni. *J. Chem. Phys.* **1990**, *93* (3), 2125–2138.

(30)   Yates, J. T.; Peden, C. H. F.; Houston, J. E.; Goodman, D. W. Subsurface Penetration of Chemisorbed Hydrogen Isotopes into the Ru(0001) Crystal Surface. *Surf. Sci.* **1985**, *160* (1), 37–45.

(31)   Bai, Y.; Chen, B. W. J.; Peng, G.; Mavrikakis, M. Density Functional Theory Study of Thermodynamic and Kinetic Isotope Effects of H_2/D_2 Dissociative Adsorption on Transition Metals. *Catal. Sci. Technol.* **2018**, *8* (13), 3321–3335.

(32)   Kresse, G.; Furthmüller, J. Efficiency of Ab-Initio Total Energy Calculations for Metals

and Semiconductors Using a Plane-Wave Basis Set. *Comput. Mater. Sci.* **1996**, *6* (1), 15–50.

(33) Kresse, G.; Furthmüller, J. Efficient Iterative Schemes for Ab Initio Total-Energy Calculations Using a Plane-Wave Basis Set. *Phys. Rev. B* **1996**, *54* (16), 11169–11186.

(34) Blöchl, P. E. Projector Augmented-Wave Method. *Phys. Rev. B* **1994**, *50* (24), 17953–17979.

(35) Kresse, G.; Joubert, D. From Ultrasoft Pseudopotentials to the Projector Augmented-Wave Method. *Phys. Rev. B* **1999**, *59* (3), 1758–1775.

(36) Perdew, J. P.; Wang, Y. Accurate and Simple Analytic Representation of the Electron-Gas Correlation-Energy. *Phys. Rev. B* **1992**, *45* (23), 13244–13249.

(37) Henkelman, G.; Uberuaga, B. P.; Jonsson, H. A Climbing Image Nudged Elastic Band Method for Finding Saddle Points and Minimum Energy Paths. *J. Chem. Phys.* **2000**, *113* (22), 9901–9904.

(38) Kittel, C. *Introduction to Solid State Physics*, 8th ed.; Johnson, S., Ed.; John Wiley & Sons, Inc.: New York.

(39) Walters, C. F.; Poker, D. B.; Zehner, D. M.; Plummer, E. W. The Deuterium-Induced Reconstruction of Cu(100): Correlation of Surface Structures with Absolute Coverage. *Surf. Sci.* **1994**, *312* (3), L759–L766.

(40) Chorkendorff, I.; Rasmussen, P. B. The P4g or Pgg Reconstruction on Cu(100). *J. Phys. Condens. Matter* **1991**, *3* (S), S107–S110.

(41) Graham, A. P.; McCash, E. M.; Allison, W. Adsorbate Structure in the H-Induced P4g Reconstruction of the Cu(001) Surface. *Phys. Rev. B* **1995**, *51* (8), 5306–5310.

(42) Hellman, A.; Svensson, K.; Andersson, S. Hydrogen-Induced Reconstruction of Cu(100): Two-Dimensional and One-Dimensional Structures of Surface Hydride. *J. Phys. Chem. C* **2014**, *118* (29), 15773–15778.

(43) Monkhorst, H. J.; Pack, J. D. Special Points for Brillouin-Zone Integrations. *Phys. Rev. B* **1976**, *13* (12), 5188–5192.

(44) Bengtsson, L. Dipole Correction for Surface Supercell Calculations. *Phys. Rev. B* **1999**, *59* (19), 12301–12304.

(45) Neugebauer, J.; Scheffler, M. Adsorbate-Substrate and Adsorbate-Adsorbate Interactions of Na and K Adlayers on Al(111). *Phys. Rev. B* **1992**, *46* (24), 16067–16080.

(46) Bajpai, A.; Mehta, P.; Frey, K.; Lehmer, A. M.; Schneider, W. F. Benchmark First-Principles Calculations of Adsorbate Free Energies. *ACS Catal.* **2018**, *8* (3), 1945–1954.

(47) García-Diéguez, M.; Hibbitts, D. D.; Iglesia, E. Hydrogen Chemisorption Isotherms on Platinum Particles at Catalytic Temperatures: Langmuir and Two-Dimensional Gas Models Revisited. *J. Phys. Chem. C* **2019**, *123* (13), 8447–8462.

(48) Fang, W.; Richardson, J. O.; Chen, J.; Li, X.-Z.; Michaelides, A. Simultaneous Deep Tunneling and Classical Hopping for Hydrogen Diffusion on Metals. *Phys. Rev. Lett.* **2017**, *119* (12), 126001.

(49) Kyriakou, G.; Davidson, E. R. M.; Peng, G.; Roling, L. T.; Singh, S.; Boucher, M. B.; Marcinkowski, M. D.; Mavrikakis, M.; Michaelides, A.; Sykes, E. C. H. Significant Quantum Effects in Hydrogen Activation. *ACS Nano* **2014**, *8* (5), 4827–4835.

(50) Alecu, I. M.; Zheng, J.; Zhao, Y.; Truhlar, D. G. Computational Thermochemistry: Scale Factor Databases and Scale Factors for Vibrational Frequencies Obtained from Electronic Model Chemistries. *J. Chem. Theory Comput.* **2010**, *6* (9), 2872–2887.

(51) Tatarkhanov, M.; Rose, F.; Fomin, E.; Ogletree, D. F.; Salmeron, M. Hydrogen Adsorption

on Ru(001) Studied by Scanning Tunneling Microscopy. *Surf. Sci.* **2008**, *602* (2), 487–492.

(52)   Lee, G.; Sprunger, P. T.; Okada, M.; Poker, D. B.; Zehner, D. M.; Plummer, E. W. Chemisorption of Hydrogen on the Ag(111) Surface. *J. Vac. Sci. Technol. A Vacuum, Surfaces, Film.* **1994**, *12* (4), 2119–2123.

(53)   Lee, G.; Plummer, E. W. High-Resolution Electron Energy Loss Spectroscopy Study on Chemisorption of Hydrogen on Cu(111). *Surf. Sci.* **2002**, *498* (3), 229–236.

(54)   Lui, K. M.; Kim, Y.; Lau, W. M.; Rabalais, J. W. Quantitative Determination of Hydrogen Adsorption Site on the Pt(111)-(1×1) Surface by Low Energy Ion Channeling. *Appl. Phys. Lett.* **1999**, *75* (4), 587–589.

(55)   Løvvik, O. M.; Olsen, R. A. Adsorption Energies and Ordered Structures of Hydrogen on Pd(111) from Density-Functional Periodic Calculations. *Phys. Rev. B* **1998**, *58* (16), 10890–10898.

(56)   Hagedorn, C. J.; Weiss, M. J.; Weinberg, W. H. Dissociative Chemisorption of Hydrogen on Ir(111): Evidence for Terminal Site Adsorption. *Phys. Rev. B* **1999**, *60* (20), R14016–R14018.

(57)   Fukuoka, M.; Okada, M.; Matsumoto, M.; Ogura, S.; Fukutani, K.; Kasai, T. Location of Hydrogen Adsorbed on Rh(111) Studied by Low-Energy Electron Diffraction and Nuclear Reaction Analysis. *Phys. Rev. B* **2007**, *75* (23), 235434.

(58)   Hammer, L.; Landskron, H.; Nichtl-Pecher, W.; Fricke, A.; Heinz, K.; Müller, K. Hydrogen-Induced Restructuring of Close-Packed Metal Surfaces: H/Ni(111) and H/Fe(110). *Phys. Rev. B* **1993**, *47* (23), 15969–15972.

(59)   Huesges, Z.; Christmann, K. Interaction of Hydrogen with a Cobalt(0001) Surface. *Zeitschrift für Phys. Chemie* **2013**, *227* (6–7), 881–899.

(60)   Ferrin, P.; Kandoi, S.; Nilekar, A. U.; Mavrikakis, M. Hydrogen Adsorption, Absorption and Diffusion on and in Transition Metal Surfaces: A DFT Study. *Surf. Sci.* **2012**, *606* (7–8), 679–689.

(61)   Kostov, K. L.; Widdra, W.; Menzel, D. Hydrogen on Ru(001) Revisited: Vibrational Structure, Adsorption States, and Lateral Coupling. *Surf. Sci.* **2004**, *560* (1–3), 130–144.

(62)   Ke, Z.; Lai, W.; Xie, D.; Zhang, D. H. First-Principles Potential Energy Surfaces and Vibrational States of H⁄Rh(111) at 0.25 and 1 Monolayer Coverages. *J. Appl. Phys.* **2006**, *99* (11), 113704.

(63)   Yanagita, H.; Fujioka, H.; Aruga, T.; Takagi, N.; Nishijima, M. Vibrational Spectra of Hydrogen on the Rh(111) Surface. *Surf. Sci.* **1999**, *441* (2–3), 507–514.

(64)   Lansford, J. L.; Mironenko, A. V.; Vlachos, D. G. Scaling Relationships and Theory for Vibrational Frequencies of Adsorbates on Transition Metal Surfaces. *Nat. Commun.* **2017**, *8* (1), 1842.

(65)   Lerch, D.; Klein, A.; Schmidt, A.; Müller, S.; Hammer, L.; Heinz, K.; Weinert, M. Unusual Adsorption Site of Hydrogen on the Unreconstructed Ir(100) Surface. *Phys. Rev. B* **2006**, *73* (7), 075430.

(66)   Heinz, K.; Hammer, L.; Gumler, B.; Meyer, W.; Schmidt, A. Ligand Effect in Hydrogen Adsorption on Epitaxial Nickel Films. *Z. Phys. Chem.* **2009**, *223*, 75–88.

(67)   Gladys, M. J.; Kambali, I.; Karolewski, M. A.; Soon, A.; Stampfl, C.; O'Connor, D. J. Comparison of Hydrogen and Deuterium Adsorption on Pd(100). *J. Chem. Phys.* **2010**, *132* (2), 024714.

(68)   Zemlyanov, D. Y.; Smirnov, M. Y.; Gorodetskii, V. V. HREELS Characterization of Hydrogen Adsorption States on the Pt(100)-(Hex) and (1 × 1) Surfaces. *Catal. Letters* **1997**,

43 (1–2), 181–187.

(69) Vesselli, E.; Baraldi, A.; Bondino, F.; Comelli, G.; Peressi, M.; Rosei, R. Coverage-Dependent Hydrogen Adsorption Site Determination on Rh(100) by High-Resolution Core-Level Spectroscopy. *Phys. Rev. B* **2004**, *70* (11), 115404.

(70) Jung, S. C.; Kang, M. H. Effect of Hydrogen on the Surface Relaxation of Pd(100), Rh(100), and Ag(100). *Phys. Rev. B* **2005**, *72* (20), 205419.

(71) Michelsen, H. A.; Rettner, C. T.; Auerbach, D. J. The Adsorption of Hydrogen at Copper Surfaces: A Model System for the Study of Activated Adsorption. *Surf. React.* **1994**, *34*, 185–237.

(72) Healey, F.; Carter, R. N.; Worthy, G.; Hodgson, A. Endothermic Dissociative Chemisorption of Molecular D_2 on Ag(111). *Chem. Phys. Lett.* **1995**, *243* (1–2), 133–139.

(73) Küchenhoff, S.; Brenig, W.; Chiba, Y. Vibrationally Assisted Sticking, Tunneling and Isotope Effect for Hydrogen on Cu Surfaces. *Surf. Sci.* **1991**, *245* (3), 389–400.

(74) Halstead, D.; Holloway, S. The Influence of Potential Energy Surface Topologies on the Dissociation of H_2. *J. Chem. Phys.* **1990**, *93* (4), 2859–2870.

(75) Rasmussen, P. B.; Holmblad, P. M.; Christoffersen, H.; Taylor, P. A.; Chorkendorff, I. Dissociative Adsorption of Hydrogen on Cu(100) at Low Temperatures. *Surf. Sci.* **1993**, *287–288*, 79–83.

(76) Ma, X.; Xin, H. Orbitalwise Coordination Number for Predicting Adsorption Properties of Metal Nanocatalysts. *Phys. Rev. Lett.* **2017**, *118* (3), 036101.

(77) Hamza, A. V.; Madix, R. J. Dynamics of the Dissociative Adsorption of Hydrogen on Ni(100). *J. Phys. Chem.* **1985**, *89* (25), 5381–5386.

(78) Pati, S.; Jat, R. A.; Mukerjee, S. K.; Parida, S. C. Hydrogen Isotope Effect on Thermodynamic and Kinetics of Hydrogen/Deuterium Absorption–Desorption in $Pd_{0.77}Ag_{0.10}Cu_{0.13}$Alloy. *J. Phys. Chem. C* **2015**, *119* (19), 10314–10320.

(79) Zhou, C.; Wu, J.; Nie, A.; Forrey, R. C.; Tachibana, A.; Cheng, H. On the Sequential Hydrogen Dissociative Chemisorption on Small Platinum Clusters: A Density Functional Theory Study. *J. Phys. Chem. C* **2007**, *111* (34), 12773–12778.

(80) Hong, S.; Rahman, T. S.; Heid, R.; Bohnen, K. P. Insights from Calculated Phonon Dispersion Curves for an Overlayer of H on Pt(111). *Surf. Sci.* **2005**, *587* (1–2), 41–49.

(81) Durman, R.; Jayasooriya, U. A.; Kettle, S. F. A.; Mahasuverachai, S.; Mortimer, R.; Norrby, L. J. Factor Group Splitting and Dispersion on Internal Vibrational Modes: A Qualitative Discussion. *J. Chem. Phys.* **1984**, *81* (12), 5247–5251.

(82) Kozlov, S. M.; Aleksandrov, H. A.; Neyman, K. M. Energetic Stability of Absorbed H in Pd and Pt Nanoparticles in a More Realistic Environment. *J. Phys. Chem. C* **2015**, *119* (9), 5180–5186.

(83) Almithn, A. S.; Hibbitts, D. D. Supra-Monolayer Coverages on Small Metal Clusters and Their Effects on H_2 Chemisorption Particle Size Estimates. *AIChE J.* **2018**, *64* (8), 3109–3120.

(84) Ciobica, I. M.; Kleyn, A. W.; Van Santen, R. A. Adsorption and Coadsorption of CO and H on Ruthenium Surfaces. *J. Phys. Chem. B* **2003**, *107* (1), 164–172.

(85) Skúlason, E.; Karlberg, G. S.; Rossmeisl, J.; Bligaard, T.; Greeley, J.; Jónsson, H.; Nørskov, J. K. Density Functional Theory Calculations for the Hydrogen Evolution Reaction in an Electrochemical Double Layer on the Pt(111) Electrode. *Phys. Chem. Chem. Phys.* **2007**, *9* (25), 3241–3250.

(86) Greeley, J.; Mavrikakis, M. A First-Principles Study of Surface and Subsurface H on and

in Ni(111): Diffusional Properties and Coverage-Dependent Behavior. *Surf. Sci.* **2003**, *540* (2–3), 215–229.

(87)   Johansson, M.; Skúlason, E.; Nielsen, G.; Murphy, S.; Nielsen, R. M.; Chorkendorff, I. Hydrogen Adsorption on Palladium and Palladium Hydride at 1bar. *Surf. Sci.* **2010**, *604* (7– 8), 718–729.

(88)   Bhatia, B.; Sholl, D. S. Chemisorption and Diffusion of Hydrogen on Surface and Subsurface Sites of Flat and Stepped Nickel Surfaces. *J. Chem. Phys.* **2005**, *122* (20), 1–8.

For Table of Contents Only